ISTANBUL TECHNICAL UNIVERSITY ★ INSTITUTE OF SCIENCE AND TECHNOLOGY

THERMAL PROPERTIES AND MICROSTRUCTURAL CHARACTERIZATION OF NON-DOPED AND ERBIUM DOPED BINARY GeO_2-V_2O_5 GLASSES

M.Sc. Thesis by
Deniz YILMAZ

Department : Advanced Technologies

Programme : Materials Science and Engineering

OCTOBER 2010

İSTANBUL TECHNICAL UNIVERSITY ★ INSTITUTE OF SCIENCE AND TECHNOLOGY

THERMAL PROPERTIES AND MICROSTRUCTURAL CHARACTERIZATION OF NON-DOPED AND ERBIUM DOPED BINARY GeO_2-V_2O_5 GLASSES

M.Sc. Thesis by
Deniz YILMAZ
(521081004)

Date of submission : 13 September 2010
Date of defence examination: 01 October 2010

Supervisor (Chairman) : Prof. Dr. M. Lütfi ÖVEÇOĞLU (ITU)
Members of the Examining Committee : Prof. Dr. Süheyla AYDIN (ITU)
Prof. Dr. Gönül ÖZEN (ITU)

OCTOBER 2010

İSTANBUL TEKNİK ÜNİVERSİTESİ ★ FEN BİLİMLERİ ENSTİTÜSÜ

KATKISIZ VE ERBİYUM KATKILI İKİLİ GeO2-V2O5 CAMLARININ TERMAL ÖZELLİKLERİ VE MİKROYAPISAL KARAKTERİZASYONU

YÜKSEK LİSANS TEZİ
Deniz YILMAZ
(521081004)

Tezin Enstitüye Verildiği Tarih : 13 Eylül 2010
Tezin Savunulduğu Tarih : 01 Ekim 2010

Tez Danışmanı : Prof. Dr. M. Lütfi ÖVEÇOĞLU (İTÜ)
Diğer Jüri Üyeleri : Prof. Dr. Süheyla AYDIN (İTÜ)
Prof. Dr. Gönül ÖZEN (İTÜ)

EKİM 2010

FOREWORD

Firstly, I would like to express my greatest gratitude and thanks to my supervisor Prof. Dr. M. Lütfi ÖVEÇOĞLU for his guidance and help during both my graduate studies and my dissertation work.

I am very grateful to Res. Assist. Demet TATAR for her everlasting support and guidance throughout my dissertation work. I am also grateful to Res. Assist. Hasan GÖKÇE and Res. Assist. Ahmet Umut SÖYLER for their great help in my experimental work.

I am thankful to the members of the Particulate Materials laboratories, namely Res. Assist. Selim COŞKUN, Şeyma DUMAN, Mithat Cem ELBİZİM, Alper EVİRGEN, Aziz GENÇ, Nida YILDIZ USLU, Sezen Seda YAKAR and Hatice Kübra YUMAKGİL for their support and contributions to my studies. I am also thankful to Çiğdem ÇAKIR KONAK for her patience and help during my electron microscopy investigations.

I am deeply grateful to my parents Ayten YILMAZ and Servet YILMAZ and my sister Derya YILMAZ TURHAN for their understanding, companionship, support and advices, this dissertation work could not have been completed without their positive interference

OCTOBER 2010

Deniz Yılmaz

B.S Physics

TABLE OF CONTENTS

Page

ABBREVIATIONS

GeO_2	**:** Germanium dioxide
V_2O_5	**:** Divanadyum pentaoxide
Er_2O_3	**:** Dierbium trioxide
DTA	**:** Differential Thermal Analysis
XRD	**:** X-Ray Diffraction
SEM	**:** Scanning Electron Microscope
EDS	**:** Energy Dispersive Spectrometry
°C	**:** Celsius
% wt	**:** Weight Percentage

LIST OF TABLES

Page

LIST OF FIGURES

Page

THERMAL PROPERTİES AND MİCROSTRUCTURAL CHARACTERİZATİON OF NON-DOPED AND ERBIUM DOPED BİNARY GeO_2 –V_2O_5 GLASSES

SUMMARY

Glass forming ability of germanium oxide was known for a long time but the detailed studies have been conducted in the last decades. The transmission ability in wide light spectrum allows these glasses to be used as optical applications such as upconversion lasers, linear and non-linear optical lasers.

The germanate glasses exhibit great optical properties when they are combined with heavy metal oxides. Among the borate and fluoride glasses the germanate glasses have smaller phonon energies, higher refractive index and lower light scattering properties. Therefore, they are promising materials for active and passive optical fibers, photonic and optoelectronic devices.

Understanding the nucleation process and crystallization behaviour is important to develop and use germanate glasses on the optical devices as laser materials which are subjected to high thermal loads during to laser beam exposure and subsequently leads to crystalization.

In the this study, thermal and microstructural properties of binary GeO_2-V_2O_5 glasses were investigated using differential thermal analyzer (DTA), X-ray diffractometer (XRD) and scanning electron microscope (SEM) techniques to understand thermal behaviour and identify crystalline phase.

Non-doped and Er_2O_3 doped GeO_2 – V_2O_5 binary glasses are investigated with varying V_2O_5 content to obtain glass transition temperatures, crystallization peak temperatures and melting temperatures. In addition, effect of Er_2O_3 content on thermal behaviour of non-doped binary GeO_2 – V_2O_5 glass system are also reported. Crystalline phases on the heat-treated glass-ceramic samples are identified as α–GeO_2, β–GeO_2, $ErVO_4$,and V_2O_5.

KATKISIZ VE ERBİYUM KATKILI İKİLİ GeO_2-V_2O_5 CAMLARININ TERMAL ÖZELLİKLERİ VE MİKROYAPISAL KARAKTERİZASYONU

ÖZET

Germanyum okisidin cam yapabilme özelliği uzun bir süredir bilinmesine rağmen detaylı araştırmalar son senelerde yapılmıştır. Geniş ışık spektrumunda, geçirgenlik özelliğine sahip olması bu camların upconversion, lineer ve lineer olmayan optik lazerlerde kullanılmasına olanak tanır.

Germanat camları, ağır metal oksitlerle birleşitirildinde iyi optik özelliklere sahip olurlar. Borat ve flüorit camlar arasında germanat camları düşük fonon enerjisine, yüksek kırılma indisine ve düşük ışık saçma özelliğine sahiptir. Bu nedenle, akif ve pasif optik fiberler, fotonik ve optoelektronik cihazlar tasarımların üretilmesine olanacak tanır.

Çekirdeklenme prosesini ve kristallizasyon davranışını incelemek, lazer demetinden dolayı ve yüksek termal yükten kristalleşen optik araçlarda germanat camının araştırılması ve kullanılması için önemlidir.

Bu çalışmada, ikili GeO_2-V_2O_5 camlarının termal ve mikroyapısal özellikleri, termal davranışlarının incelenmesi ve kristaller fazlarının belirlenmesi için diferansiyel termal analiz (DTA), X-ışınları kırınımı (XRD) ve taramalı elektron mikroskopu (SEM) yöntemleri kullanılarak araştırılmıştır.

Katkısız ve Er_2O_3 katkılı GeO_2 – V_2O_5 ikili camları, değişen V_2O_5 katkısı ile cam geçiş sıcaklıkları, kristallizasyon tepe sıcaklıkları ve erime sıcaklıklarını elde etmek amacı ile incelenmiştir. Bunlara ek olarak, Er_2O_3 katkısının termal davranışı, ikili GeO_2 – V_2O_5 cam sistemi içinbildirilmiştir. Isıl işlem görmüş cam-seramik numunelerin kristal fazları α–GeO_2, β–GeO_2, $ErVO_4$ and V_2O_5 olarak belirlenmiştir.

1. INTRODUCTION

In the last decade, germanate glasses have drawn great attention since they exhibit good anti radiation and infrared-transmittance character, thermal properties and ability for high concentration doping features (Lin et al.,2009; M. Yamane and Y. Asahara, 2000; Walsh et al., 2006; Zhang et al., 2010; Bayya et al., 2006; Margaryan and Piliavin, 1993). Despite these properties it is possible to fabricate germanium oxide based glasses with numerous optical spectroscopic properties through doping with rare earth elements since GeO_2 glasses has low phonon energy. Furthermore they are promising materials for laser luminescent applications as they have high quantum efficiency of luminescence (Hussain et al.,2001; Klimesz et al., 2007).

Addition of transition metal ions such as V, Mo, Fe and Co into the glass network provides semiconducting features due to presence of the transition metal ions in different valance states (Sankarappa et al.,2008; El-Mallawany, 1999; El-Deen, 2000). Electronically conducting structure of transition metal ion based glasses make them desirable for many applications. Vanadium based glasses have been studied in different host glasses but there exist very limited studies carried on the binary GeO_2-V_2O_5 glass system (Khawaja et al.,1985; Kobayasbhi, 2002; Mukherjee et al.,1996; Elsharkawy et al., 1984; Mukherjee et al.,1993; Memon 1998; Marinov, 1975; Khan et al.,1984). In addition, the present literature generally reports on the electrical conductivity and ultrasonic properties of these glasses.

Thermal stability of the glasses plays a major role on possible technical applications (Wang et al., 2010; Santos et al., 2009; Wang et al.,2003). Therefore thermal analysis of the fabricated glasses should be carefully investigated in order to study crystallization mechanisms (Öveçoğlu et al.,2007; Ozen et al.,2008; Tatar et al., 2008; Öveçoğlu et al.,2005). In the present study, characterization investigations were carried out on the $GeO_2 - V_2O_5 - Er_2O_3$ glass system to analyze thermal properties and microstructural characterization. Er3+ ion was selected as the dopant ion for infrared and visible upconversion lasers application.

Vanadium germanate glasses were prepared having the compositions of (1-x)GeO_2 – x V_2O_5 (x= 0.30,0.42 and 0.60 in molar ratio) and also the same compositions doped with 0.5 % mol Er_2O_3 and 1 % mol Er_2O_3. Thermal analyses of the glasses were performed using differential thermal analysis (DTA) and microstructural characterization investigations were carried out with x-ray diffraction (XRD) and scanning electron microscopy (SEM).

2. GERMANIUM OXIDE BASED GLASSES

2.1 Germanium Oxide

Germanium monoxide, GeO, and germanium dioxide, GeO_2 are the two stable binary compounds constituted by the Ge and O elements. GeO is stable at room temperature and between 600-1400°C it becomes unstable and decomposes to Ge and GeO_2 (Margaryan and Piliavin, 1993)

Germanium dioxide has a polymorphic structure which is found at glass-forming (amorphous), rutilelike (tetragonal), α-quartz like, and β-quartz like and chalcedonic (hexagonal) form. As seen in pressure-temperature (P-T) phase diagram which is demonstrated in Figure 2.1, the rutile-like tetragonal form of GeO_2 is stable below 1000°C and the quartz like hexagonal form of GeO_2 is stable between 1049-1116°C while the tetragonal form GeO_6 transforms into the hexagonal form GeO_4 at 1049°C. (Margaryan and Piliavin, 1993) and remains stable at that temperature. Therefore, a single crystal with a α-quartz like structure grows during cooling from the liquid state or from a solution at ambient pressure (K. Niwa et al., 2009). Monocrystalline quartz like structures of germanium dioxide (α-GeO_2) are considered for expected piezoelectric applications. Because of the absence in nature and growth difficulties in laboratory conditions , the piezoelectric constants of α-GeO_2 could not be investigated (D. V. Balitsky et al., 1996*)*. On the other hand, rutile-type GeO_2 have much greater stiffness than the quartz-like structures and they are easier to growth (A. Trukhin et al., 2005).

Obtaining efficient visible luminescence from the indirect gap element at semiconductors Si or Ge has been the subject of several recent investigations on optical, structural and electronic properties (Amato et al, 1997). Germanium dioxide (GeO_2) is one of the dielectric oxides that are promising materials for optical devices such as optical wave guides for integrated optical systems (Calas et al., 2007)

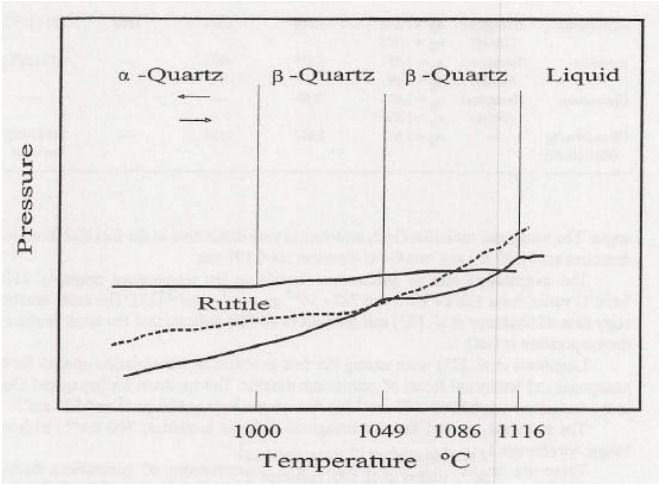

Figure 2.1 : Polymorphic Transition of GeO_2 with pressure and temperature (Margaryan and Piliavin, 1993).

Balitsky et al.,1997 succeeded on crystal growth of prismatic α-GeO_2 crystals and many of them reside at solution-wall boundary. They also accomplished on nucleating thin dendrite crystals of α-GeO_2 on the surface of the solution (Balitsky et al., 1997).

2.2 Germanium Oxide Glasses

Silicate, borate, germanate, vanadate or telluride systems are used as important components of various devices in optic, electronics and opto-electronics fields (Yamane and Asahara, 2000). Although germanate , vanadate and telluride systems are not used in mass production due to their high cost of raw materials, their unique properties make them desirable in various field of applications(M. Yamane and Y. Asahara, 2000). Among oxide glasses, SiO_2, GeO_2, B_2O_3, and P_2O_5 are known as good glass network formers which can develop three dimensional random network and can form glass by itself (Doremus,1994).

Figure 2.2 shows GeO_2 single component glass forms of three dimensional network of Ge-O-Ge bonds such as silica glass. Although GeO_2 glasses exhibit good chemical durability and have similar properties with silicate glasses, they are not used extensively. However, for special applications like an infrared transmitting glass and ultra-low-loss optical fiber the germanate glass has received attraction due to its higher infrared transmission (Yamane and Asahara, 2000; Margaryan and Piliavin, 1993).

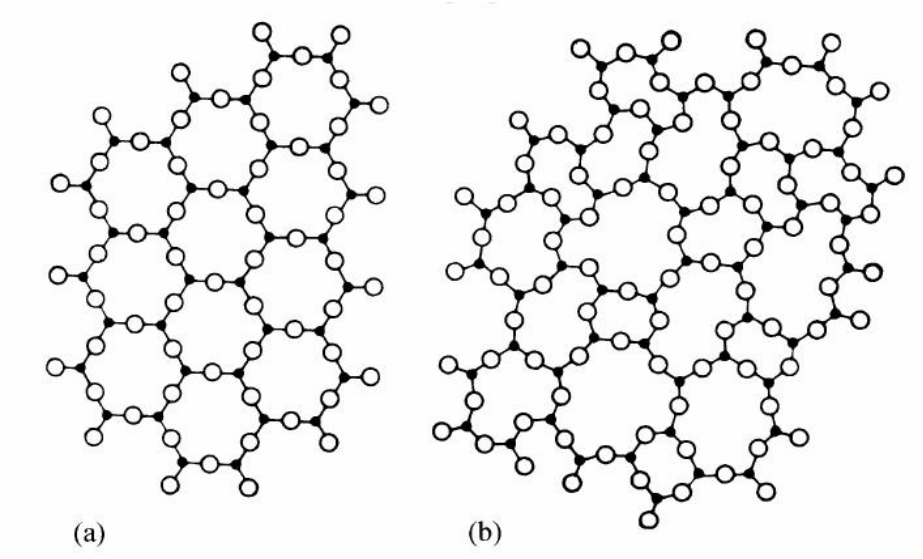

Figure 2.2 : Two dimensional illustration of crystal (a) and glass (b) arrangement (Yamane and Asahara, 2000).

Silicon dioxide and germanium dioxide share quite a few common properties (Doremus,1994). They both demonstrate polymorphism in the case of crystalline state (Shelby,2005; Margaryan and Piliavin, 1993; Prakapenka et al.,2003). The familiar α-quartz polymorph of SiO_2 is mirrored by an α-quartz-like GeO_2 polymorph, while rutile-structured stishovite SiO_2 is mirrored by rutile-like argutite GeO_2. (Trukhin,2009). As seen in Figure 2.3 the structure of rutile like GeO_2 consists of (GeO_6) octahedra that each oxygen is linked to three germanium ions and the structure of quartz like GeO_2 is formed by (GeO_4)-tetrahedra which shares corners for forming a three dimensional network (Wang et al., 2001). Compared with silicate glasses as host materials, germanate glasses have good anti-radiation and infrared transmittance characters due to the larger size and heavier mass of germanium compared to silicon (Lin et al.,2007). Consequences of heavier mass of tellurium atom among common oxide glass tellurite glass has the lowest phonon energy but at the same time it has larger refractive index which could result in a larger radiative transition rates of rare-earth ions compared to germanate glass (Sun et al.,2004). On the other hand germanate glasses have more chemical durability and higher mechanical stabilities than fluoride, oxyfluoride and sulfide glasses (Lin et al.,2007; Su et al. 2006). Recent studies have shown that germanate glasses have ability for high concentration doping (Lin et al. 2007; Su et al.2006). Moreover, germanate

glasses possess lower phonon energy, which leads to lower non radiative losses of rare earth and higher luminescence efficiency (Klimesz et al., 2007).

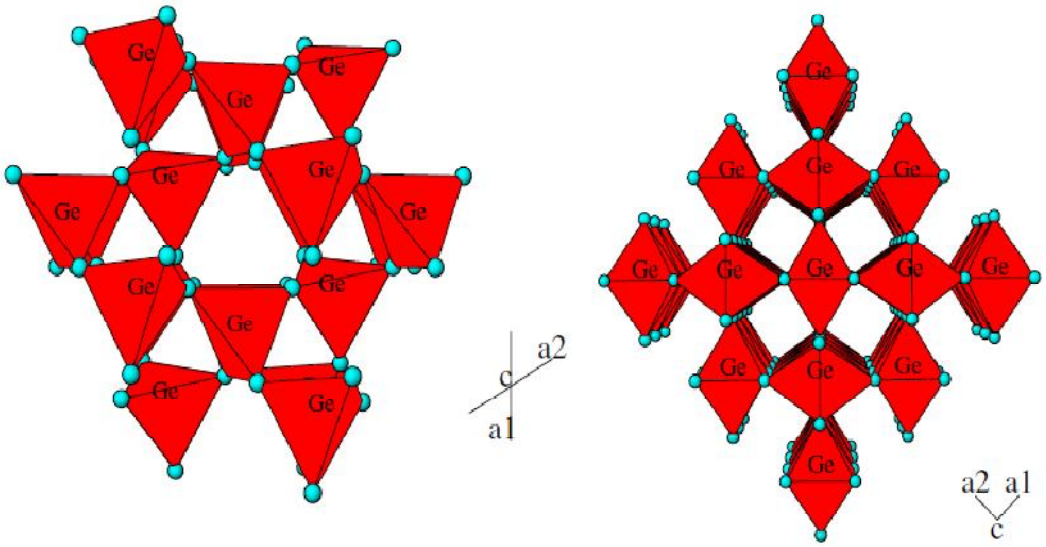

Figure 2.3: Projection of the α-quartz-like structure (left) and rutile-like structure (right) on the (001) plane (Micoulaut et al.,2006)

Alkali germanates are one of the archetypes of oxide liquids and glasses whose properties generally controlled by highly interconnected networks of small, tri- or tetravalent cations with low oxygen coordination numbers(Peng and Stabins, 2007). Among alkali borate, silicate and germanate systems, some thermophysical properties show variation with increasing alkali oxide content. Addition of modifier oxide M_aO_b to the pure vitreous germania formed by corner- sharing between tetrahedral GeO_4 units, cause effect on thermophysical properties (such as glass transition temperature, density, viscosity, for example) and they present maxima or minima different from the silicate glasses (Peng and Stebbins, 2007; Henderson, 2007; Du et al., 2007). This behavior is known as a germanate anamoly and anamoly maximum shows variation upon the nature of alkali oxide; for example for (Li_2O) anomaly maxima occurs at 20 mol% , for (Na_2O) 15 mol%, (K_2O) 9 mol% , for (Rb_2O) 15 mol% and for (Cs_2O) 17.5 mol%. (Henderson, 2007). Two main models were offered for explaining germanate anamoly, most widely accepted model is which proposed by Ivanov and Evstropiev and murthy and Ip, claimed that germanate anamoly based on to changing coordination of Ge from 4-fold (^{IV}Ge) to 6-fold (^{VI}Ge) (Henderson, 2007). With increasing alkali content, the surplus oxygen introduce to germanate network which need to be accomodate. These additional

oxygen caused structural changes as occuring variation on composition in the network. As shown in Figure 2.4, the additional oxygen may be incorporated into the network as non-bridging oxygens (NBOs) by breaking oxygen bridges (Fig. 2.4(b)) or as seen in Figure 2.5(c) it may caused to conversion of germanium atoms a lower coordination (^{IV}Ge) to higher coordination (^{VI}Ge). And also it may be incorporated by the conversion of germanium atoms from a lower coordination to a higher coordination (Fig. 2.4(c) shows the conversion of a GeO_4 unit to a GeO_6 unit) (Hannon et al., 2007). With low alkali oxide addition formation of GeO_6 units is becomes dominant while with the higher modifier contents, the formation of NBOs (non-bridging oxygen) become dominant (Hannon et al., 2007; Handerson et al., 2007). Until the maximum were observed on the physical properties, GeO_4 tetrahedra convert to GeO_6 octahedra, followed by a conversion of ^{VI}Ge back to ^{IV}Ge beyond anamoly.

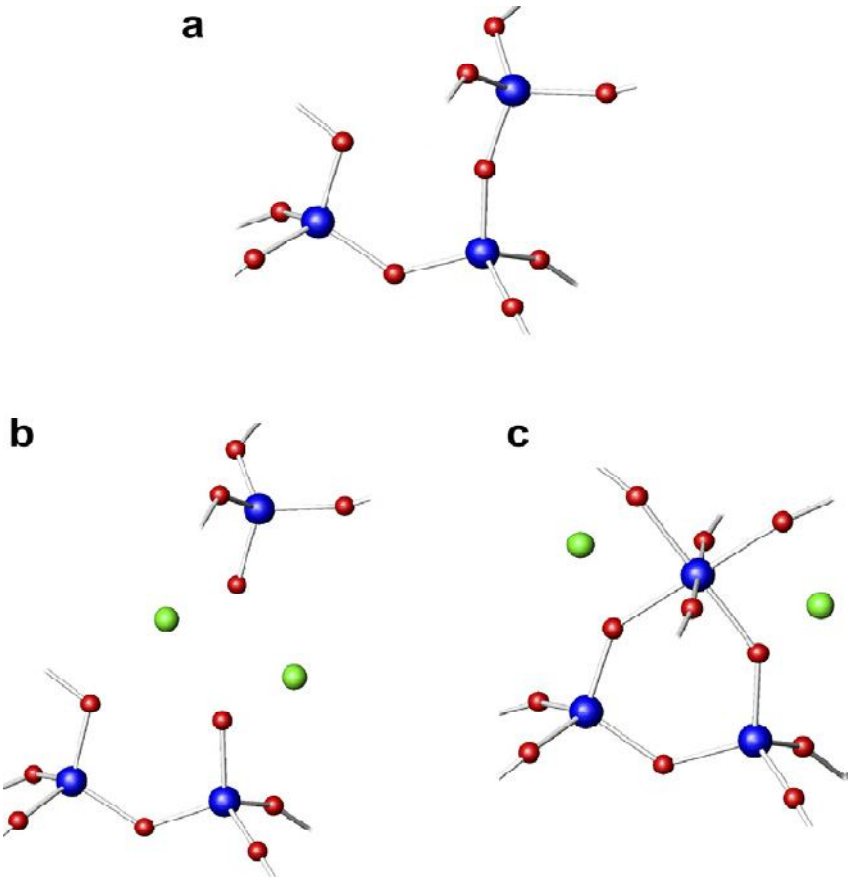

Figure 2.4 : Illustration of coordination change on alkali germanate glasses: (a) Pure GeO_2 glass which is formed by [GeO_4] tetrahedral, (b) alkali germanate glass which has two bridging and two non-bridging atoms per germanium atom, (c) alkali germanate glass which is formed by [GeO_4] tetrahedra and [GeO_6] octahedral (Hannon et al., 2007).

Bonding of oxygen atom in the network in germanium alkali oxide systems can be expressed by Equation (2.1) where oxide atoms bond with germanium tetrahedra and formation of either GeO_6 or GeO_5 and no non-bridging oxygens occur (Du et al., 2007).

$$Na_2O + {}^{[4]}GeO_{4/2} = ({}^{[6]}GeO_{6/2})^{2-} + 2Na^{+} \quad \textbf{(2.1)}$$

Formation of non-bridging oxygen in the network in germanium alkali oxide systems can be expressed by the Equation (2.2) where high amount of alkali content forces most or all of the GeO_6 or GeO_5 transform back to GeO_4 tetrahedra with non-bridging oxygen (Du et al., 2007).

$$Na_2O + {}^{[4]}GeO_{4/2} = {}^{[4]}GeO_{3/2}O^{-} + Na^{+} \quad \textbf{(2.2)}$$

Since GeO_2 is a well-known glass-former chemical compound (Nie et al., 2007), when GeO_2 is added to the glass system, thermal stability of the oxide systems can be increased and thus prevention of crystallization is achieved. However, Nie et al. (2007) observed in their studies that GeO_2 acts totally different in bismuth-borate glasses and it decreases ΔT temperature difference in these glasses which shows that GeO_2 cannot prevent crystallization in these glass compositions.

2.3 Rare earth elements and effects on the glasses

Rare-earth doped materials have drawn great attention especially for designing photonic devices including solid-state three-dimensional color displays, infrared pumped visible lasers, high resolution printing, sensors and they are investigated extensively. Among of many-rare-earth element systems, erbium doped glass systems have been studied extensively, due to their attracted features such as luminescence lifetime, emission bandwidth and upconversion efficiency (Mortier et al., 2001; Gouveia-Neto et al., 2008). in the rare-earth doped glass system, non-radiative losses or cut-off optical phonon energies should be kept small to improve intensity of the radiative emission (luminescence). The fluoride glass systems have low cut-off optical phonon energy whereas show bad chemical durability and oxide glass system show better chemical durability and better mechanical properties while have high cut-off optical phonon energy. Therefore, oxyflouride glass system can be investigated for both physical and optical properties of these glass systems (Kassab et al., 2007).

When the glass system doped with rare-earth elements like Er^{3+}, Tm^{3+}, Eu^{3+}, it is important to investigate stability of un-doped glass in order to prepare same doped glasses (Lezal et al., 2001). Er^{3+} doped tellurite glass shows good stimulated emission properties among the other glass hosts but these glass systems have low thermal stability and their ambiguity on upconverison luminescence, thus it obstructs them to be applied in industrial designs (Nie et al., 2007).

Upconversion lasers diode has been investigated widely because of promising designs like under-water optical fibers, optical data storage, sensors and infrared excited visible lasers where rare-earth ions excited (Figure 2.5) in the transparent hosts with infrared laser (Joubert, 1999). For an activator in upconversion process Er^{3+} ions are one of mostly used rare-earth ion. Although, the rare-earth element takes a significant role in upconversion lasers, the host choice is also important because glass host dominates most of the spectroscopic properties (Zhang et al., 2008).

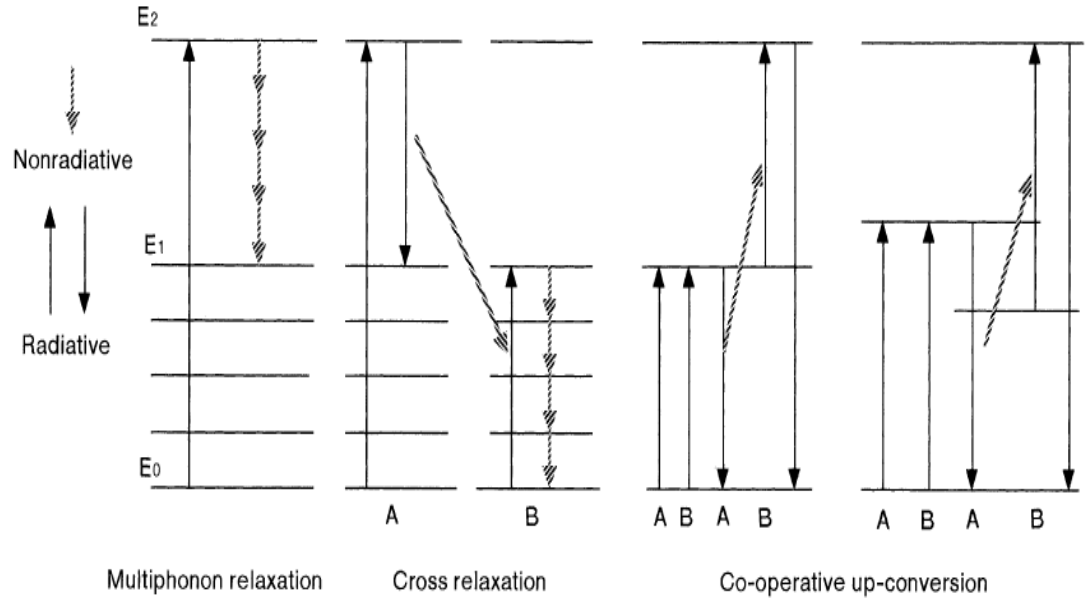

Figure 2.5 : Illustration of relaxation phenomenon of rare-earth elements (Yamane and Asahara, 2000).

When GeO_2-based glasses are doped with rare earth elements which have low phonon energy, they gain numerous optical spectroscopic properties (Mortier, 2003, Gouveia-Neto et al., 2008). Due to their lower phonon energy, they show high quantum efficiency of luminescence and they are attractive as laser and luminescent applications (Klimesz et al., 2008).

2.4 Transition Metal Ion Containing Glasses

The oxide glasses containing transition metal ions (TMI) such as V, Mo, Fe and Co have become very attractive because of their semiconducting properties, which arise from the presence of TMI in multivalent states (Kumar et al., 2008). Their electronically conducting structure explained by single phonon assisted hoping of the electrons between the multivalent states of TMIs. Binary and ternary phosphate, borate and tellurite glasses containing alkali and TMI and alkaline and TMI have been reported for dc and ac electrical conductivity (Kumar and Sankarappa, 2008). These glasses when doped with rare earth ions become useful for optical applications because they enhance their optical properties such as refractive index, optical band gap and laser amplification (Kumar et al., 2007). On the other hand, the ac conductivity studies of different rare earth ions doped binary tellurite glasses revealed that the conductivity shows decrease with doping rare earth ions. The reason of this conductivity decreasing attributed to the slow mobility of rare earth ions due to their heavy mass (Sungping et al.,2006)

Transition metal ions in oxide glasses usually have more than one valence state, such as V^{4+} and V^{5+}. Therefore, there are several studies on V_2O_5 based glasses which take interest with its conduction mechanism and glass structure. Conduction mechanism occurs by transfer of the electron low to high valance state. During the electron transfer, electron and distortion move together as a whole. Among vanadate glasses, lead vanadate glass is one of the widely investigated glass in semiconducting glasses because its wider glass-forming region is in the phase diagram and has possible technological application in threshold switching, electrical threshold and optical switching devices (Saddeek et al., 2004).

2.5 Binary Vanadium Germanate Glasses

The oxide glasses containing transition metal ions has been studied widely but there is so limited literature on the binary GeO_2-V_2O_5 glass system and as far as is known there are no studies of vanadium germanate glasses in the last decade. The literature on that binary glass system generally is about the electrical conductivity (Khawaja et al.,1985) and the ultrasonic investigation (Pal et al,1996)

Electrical conductivity of vanadium germanate glasses depends on existence of vanadium in different valance states and it is accepted that these materials are

electronic conductors in which transport mechanism involves between V^{4+} and V^{5+} ions. For increasing conductivity of binary glass system, several investigations were carried out and they revealed that the annealing process increases the conductivity which is attributed to annealing process change the microstructure (). The color of the sample also changes (yellowish green to brown) with annealing due to the change of vanadium valance state so it caused to increasing on absoption also (Khawaja et al.,1985). The other results of the conductivity of these glass system are increasing concentration of V_2O_5 increase conductivity also and comparasion with TeO2-V_2O_5 glass system shows that GeO_2 based glass has better conductivity (Khan et al.,1984)

3. CHARACTERIZATION TECHNIQUES

3.1 Thermal Analysis Techniques

It is important to study the thermal behavior and the crystallization mechanisms of glasses because glass materials, especially ones manufactured via controlled crystallization, are recently perceived as a new type of nonlinear optical materials. Besides, glasses are widely used as laser hosts and in fiber optics. Therefore, different techniques are used to understand and analyze the physical characteristics, structural characterizations, and the atomic arrangements observed in glasses (Brown,1998). Thermal analysis covers a group of techniques which measure physical properties of substances as a function of temperature while the substance is subjected to predefined heating or cooling programs (Speyer,1993; Hatakeyama and Lıu, 1998). There are different kinds of thermal analysis methods such as DTA, DSC, thermogravimetry, etc.

In differential thermal analysis (DTA), identical heat treatments are applied to the reference material and the substance, in order to measure the temperature difference between the substance and the reference material as a function of temperature (Hatakeyama and Quinn, 1999; Speyer,1993;Brown and Galagher,2003). On the other hand, a similar technique, differential scanning calorimetry, is based on the difference between the heat requirements of the substance and the reference material for keeping the same temperature.

Dimensional change of a sample can also be measured as a function of temperature or time with thermodilatometry (Brown,1998). Moreover, thermogravimetry and evolved-gas analysis methods can be carried out on samples to investigate additional data about material properties when the samples decompose at high temperature (adapted from Url-1). Additionally, thermoelectrometry, thermooptometry and thermomagnetometry techniques can be used to measure electrical, optical and magnetic properties of samples as a function of temperature.

3.1.1 Differantial Thermal Analysis (DTA)

In differential thermal analysis (DTA), the temperature difference between the sample and reference material is measured as a function of temperature or time. The schematic illustration of differential thermal analyzer is shown in Figure 3.1. The general components of the DTA are the furnace, temperature programmer, recording system and sample holder comprising thermocouples, sample containers and a ceramic or metallic block. In order to measure temperature difference, the thermocouples are inserted in each holder that is surrounded by a block to ensure an even heat distribution (Brown,1998; Hatakeyama and Lıu, 1998). The temperature programmer provides constant heating rates. The sample should be placed in a pyrex, silica, nickel or platinum crucible in order to prevent contamination and the reference material should be chosen as a thermally inert substance which show thermal similarity with the sample and exhibit no phase change over the temperature range of the experiment (Speyer,1993).

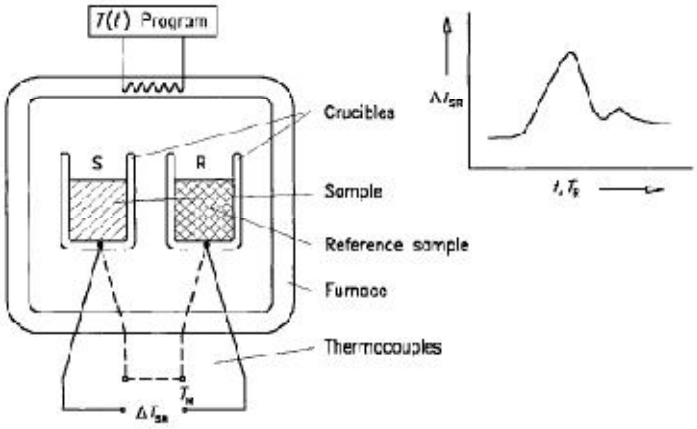

Figure 3.1: Schematic illustration of DTA (Brown,1998).

When the holders are subjected to identical heating or cooling temperature programmes, the temperatures of both the reference material and the sample change uniformly until the sample undergoes a phase change. Because if the sample undergoes any phase change, the temperature difference ($\Delta T = T_{sample} - T_{reference}$) between the sample and the reference material will be detected in consequence of the energy absorption (endothermic) or emission (exothermic). For example, during the melting of a solid, the sample will absorb heat. If the absorbed thermal energy is used for phase transformation by the sample, the temperature of the sample stays

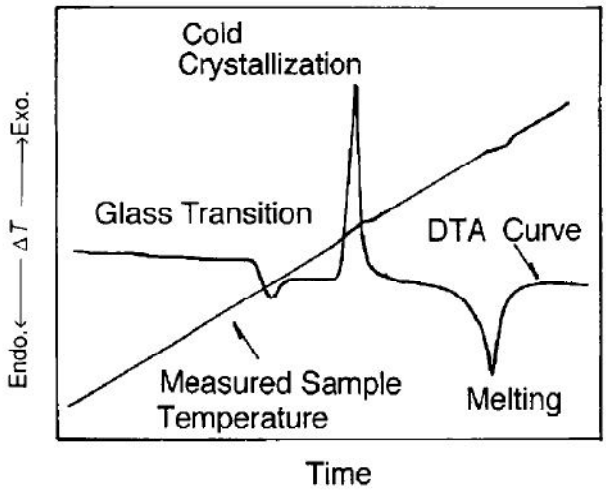

Figure 3.2 : Schematic illustration of the measured sample temperature as a function of time which is subjected to linear heating rate (Hatakeyama and Quinn, 1999).

unchanged, while the temperature of the reference material increases. In the DTA plot, the difference between the temperatures of the materials is indicated as an endotherm. In contrast, in crystallization process, the temperature of the sample will be higher than that of the reference, due to the exothermic heat of crystallization (Hatakeyama and Quinn, 1999).Therefore, the temperature scanning rate of the sample is not constant over the entire temperature range of the experiment, as seen in Figure 3.2.

3.1.2 Differential Scanning Calorimetry (DSC)

In differential scanning Calorimetry (DSC), change of the difference in the heat flow rate to the sample or to the reference material is measured while they are subjected to a temperature controlled program (Hatakeyama and Quinn, 1999; Speyer,1993). There are two main kinds of DSC commonly used:

- Heat-flux DSC
- Power compensation DSC

Basically the heat flux DSC can be defined as a technique in which the exchange of the heat through the environment and well-defined heat conduction path is measured. In heat flux DSC, the sample and the reference material are subjected to the same temperature program and put into the same furnace. The crucibles of the reference

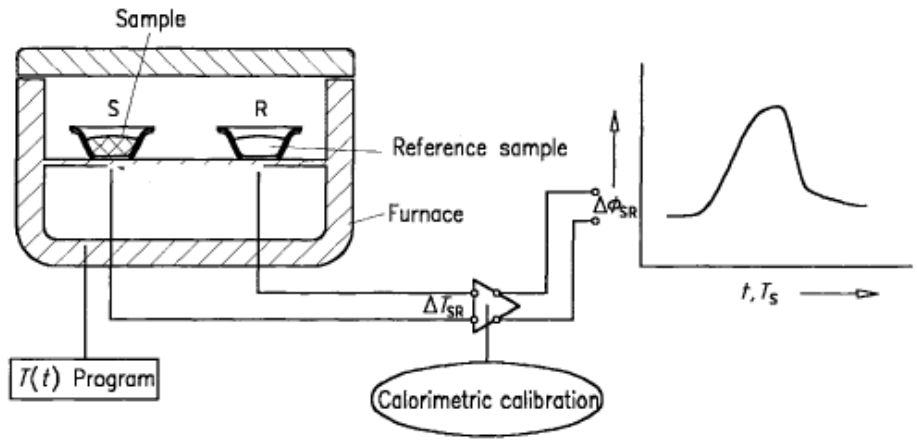

Figure 3.3 : Schematic illustration of a heat-flux DSC (Brown,1998).

and the sample are linked by a good heat flow path, therefore the temperature difference between them is small compared to DTA. The signal which is primarily measured is the temperature difference because it determines the intensity of the exchange and the resulting heat flow. Temperature difference is proportional to heat flow rate. As seen from the Figure 3.3, The heat flow rate difference is assigned by calorimetric calibration (Hatakeyama and Quinn, 1999; Speyer,1993).

In power compensation DSC technique, the temperature of the sample and the reference material are controlled by separate and identical small furnaces which have their own heating unit and temperature sensor (Brown,1998).

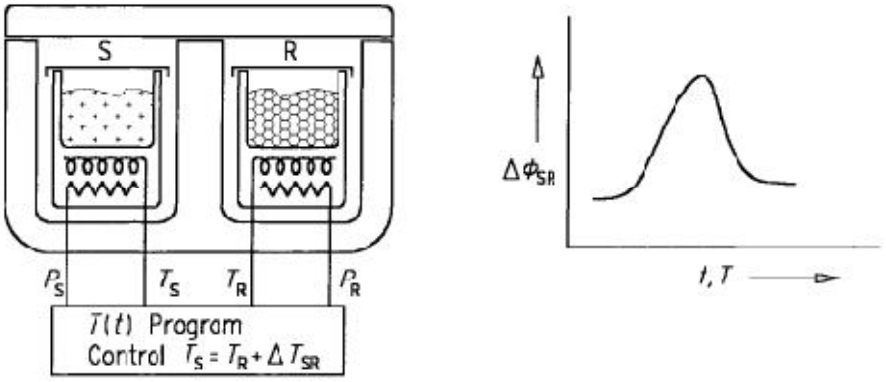

Figure 3.4 : Schematic illustration of a power compensation DSC (Brown,1998).

During the experiment, the temperature difference between the reference and the sample is required to keep at a minimum value. If a temperature difference is detected due to the phase change in the sample, the device reduces the heat input in one furnace while increasing the heat input of the other in order to maintain the zero

temperature difference. Then, the energy input or heat flow per unit time is recorded as a function of time or temperature.

3.1.3 Thermogravimetry (TG)

In thermogravimetry technique, mass change of sample is measured as a function of temperature in the scanning mode or as a function of time in the isothermal mode while the sample is subjected to either a heating or cooling temperature program(Brown,1998). This method is very important for analyzing desorption, absorption, sublimation vaporization, oxidation, reduction and decomposition which cause mass change in the sample. But there are some exceptional thermal events that cannot be analyzed with this technique, such as crystallization, melting or glass transition.

3.2. Microstructural Characterization

3.2.1. X-Rays

X-rays were discovered in 1885 by the German physicist Wilhelm Conrad Röntgen, who won the first Nobel Prize in physics in 1901 with his discovery. This breakthrough was completely coincidental and the nature of the ray was unknown at that time, therefore the ray was named as "X." Röntgen announced the exploration of the X-ray by a brief ten-page publication in the same year of his discovery. The X-ray attracted great attention from the public and the authorities because of its unique properties which are,

- Travelling in straight lines,
- Being absorbed in matter in proportion to the mass of the absorbing material,
- Darkening photographic plates
- Making shadows of the absorbing material on photosensitive paper

The last property makes the X-ray a good candidate to be used in medicine. Therefore, medical use of the X-ray was quickly adopted by Röntgen after photographing of bones through a living hand (adapted from Url-2; Cullity,1956).

After the extensive and elaborated investigations on X-rays, we know that X-rays are part of the spectrum of electromagnetic radiation with a high energy and relatively short wavelength. As seen in Figure 3.5, X-rays are located between the gamma rays and ultraviolet radiations in the electromagnetic spectrum with a wavelength of 10^{-1} to 10 Å. In X-ray diffraction, generally, X-rays with a wavelength range of 0.7 to 2.3

Å are used, because these wavelengths are comparable to the range of interatomic spacing in crystals.

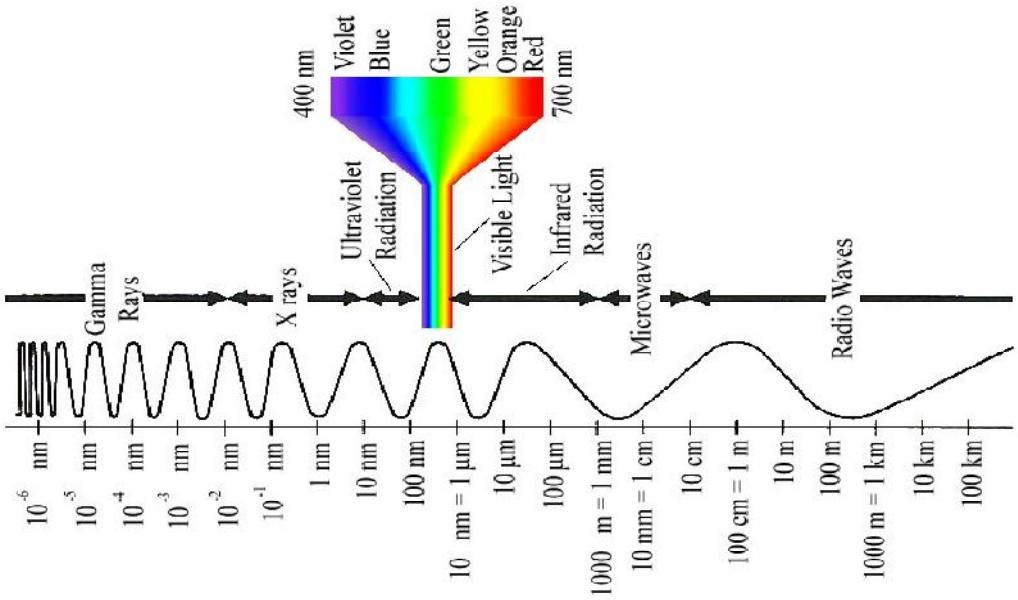

Figure 3.5 : Electromagnetic spectrum

X-rays are usually generated with the use of two different sources. One of them is synchrotron and the other one is the X-ray tubes which are the simplest and the most commonly used sources of X-rays. General physical principle of X-ray tube is based on the bombardment of the metal target (anode) with high energy electrons which are generated in and accelerated from the hot filament (cathode). The schematic view of the X-ray tube is shown in Figure 3.6. In X-ray tube, common anode materials are Cu, Mo, Fe and Cr which can be chosen in accordance with the intended wavelength of X-ray. Be windows, which are transparent to X-rays, are used to give exit to the X-ray in the direction of the specimen. Cooling water circulation is utilized in avoiding the anode melting (Chung and Smith,2000; He, 1954).

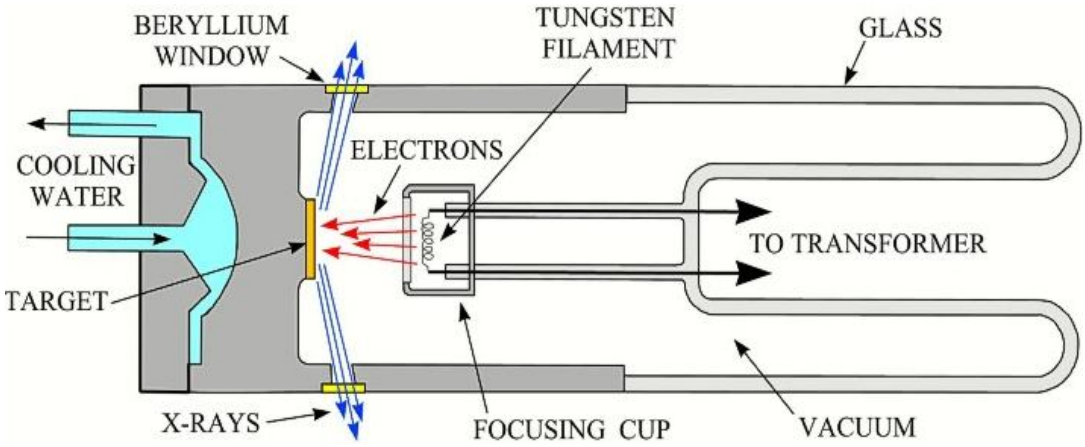

Figure 3.6 : Generation of X-rays

In Figure 3.7, the X-ray spectrum which is obtained by a typical X-ray tube is shown schematically. The spectrum has several intense peaks on continuous background. If the matter is irradiated with a beam of high-energy charged particles, X-rays are always generated. Because, the interaction between the target material and the beam may cause rapid deceleration of the impinging highly-charged electron and this process generates broadband continuous radiation which is called "Bremsstrahlung" or "white radiation."

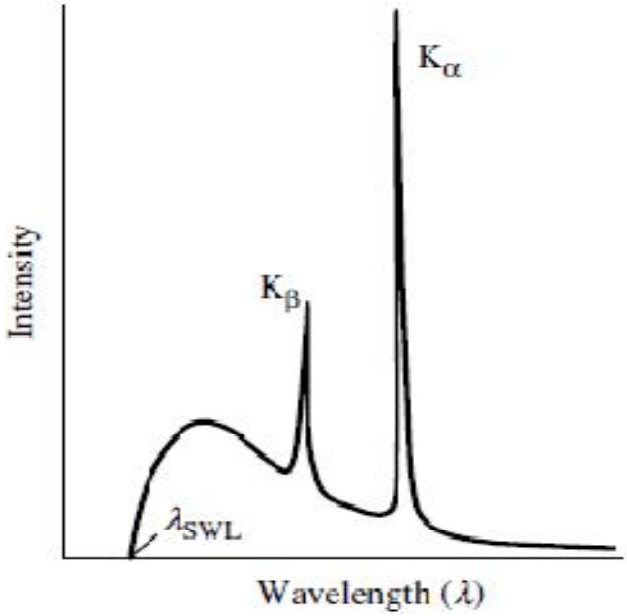

Figure 3.7 : The schematic of a typical X-ray emission spectrum (He,1954)

On the other hand, the interaction between the beam and the target may also cause an atomic electron to be removed from one of the inner orbital, creating a vacancy. This vacancy can be filled by outer-shell electrons and due to the energy difference between the two shells, X-ray generation is observed. The peaks which are superimposed with continuous spectrum are called characteristic lines and the origin of the characteristic lines is the transition of the atomic electrons between the inner and outer shells. Wavelength of these peaks depends on the nature of target materials, therefore the values of the characteristic lines differ for each target element. Atomic electron transition is shown schematically in Figure 3.8. For example, if a K-shell electron is displaced by an incoming electron and the L-shell electron is transferred to the K-shell, K_α X-ray is produced. If an M-shell electron is fills the vacancy of a K-shell electron, K_β X-ray is produced (Jenkins and Synder,1996).

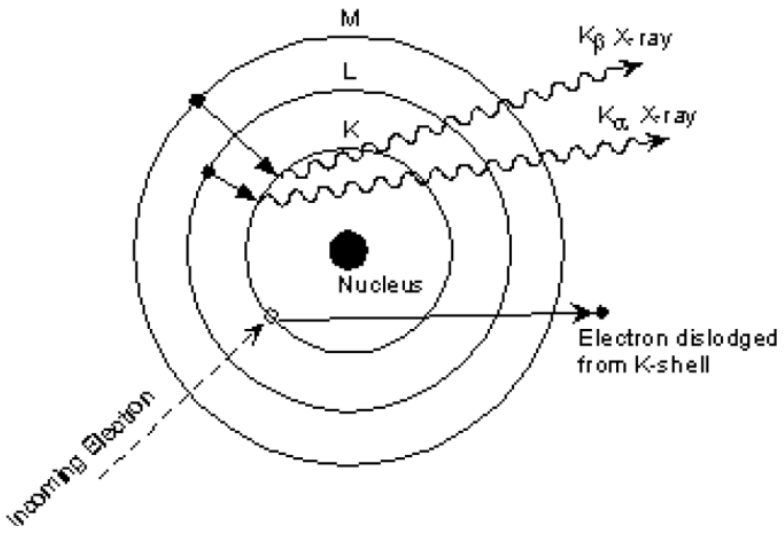

Figure 3.8 : Schematic illustrition of electronic transitions in an atom(Synder and Jerkins,1996)

3.2.1.1. Bragg's Law and X-ray Diffraction

In 1912 at the University of Munich, Max von Laue and his colleague directed a beam of X-rays at a crystal of copper sulfate and tried to get scattered beams recorded on a photographic plate. As a result of this experiment, they proved that X-rays consist of waves and the crystal comprise of the atoms which are arranged on a space lattice. Thereby the first explanation of the X-ray diffraction was introduced by Max von Laue. One year after this experiment, William Henry Bragg and his son William Lawrence Bragg found a new mathematical form of diffraction, which is a much simpler way of understanding the phenomena of diffraction from crystal. In Bragg's approximation which is schematically shown in Figure 3.9, the incident rays are assumed as in the same phase. As seen in the Figure 3.9, the incident monochromatic X-ray beams hit the crystal planes with an incident angle of θ. The beam labeled as 2, travels a distance that is |AB| + |BC| farther than the beam labeled as 1 does. Similarly, the waves which are reflected from the third plane travel a distance farther than beam 2. The distance travelled increases in correspondence with the plane number. Therefore, the waves which are reflected from the planes will be phase retarded with respect to the first wave and this causes interference between the waves. Two conclusions can be drawn from this illustration:

- Difference in the lengths of travelling paths between incident beams lead to differences in phase
- Phase differences produce changes in amplitude

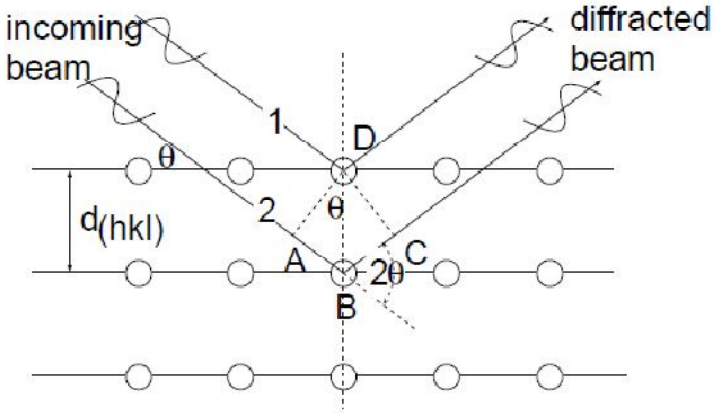

Figure 3.9 : Schematic illustration of X-ray difraction from atomic plane (adapted from Url-2)

A greater difference in path leads to a greater difference in phase, so for constructive interference, path difference must be equal to integral multiples of wavelengths (λ) of the incident radiation.

Accordingly:

$$AB + BC = n\lambda \quad (n=1,2,3,...) \tag{3.1}$$

$$\text{Since AB=BC and } sin\theta = \frac{AB}{d_{(hkl)}} \tag{3.2}$$

$$n\lambda = 2d_{(hkl)}\sin\theta \tag{3.3}$$

The equation above is called as Bragg's Law where λ is the wavelength, d is the distance between adjacent crystal planes, θ is the Bragg angle and n is an integer number, which is called "the order of reflection." Since sinθ cannot be greater than the unity, we may write

$$\frac{n\lambda}{2d} = \sin\theta < 1 \tag{3.4}$$

Therefore nλ must be less than 2d. For diffraction, smallest value of the n is 1. Therefore, the condition for diffraction at any observable angle 2θ is,

$$\lambda < 2d \tag{3.5}$$

Perhaps most widely used X-ray diffraction technique for characterizing materials is Powder XRD (X-ray Diffraction) technique. In that technique, the sample generally

used in its powder form, consisting of fine grains of single crystalline material to be studied.

The term 'powder' really means that the crystalline domains are randomly oriented in the sample. Therefore when the 2-D diffraction pattern is recorded, it shows scattering peaks corresponding to the various d spacing in the crystal lattice. The positions and the intensities of the peaks are used for identifying the underlying structure (or phase) of the material.

Powder diffraction data can be collected using either transmission or reflection geometry. The peak positions, intensities, widths and shapes all provide important information about the structure of the material.

3.2.2. Scanning Electron Microscope (SEM)

Microscopy is kind of a technique which involves the study of objects that are too small to be analyzed by the naked eye. Electron microscopy use the wave nature of rapidly moving electrons for examine and observed to heterogeneous organic and inorganic material on a nanometer(nm) and micrometer (μm) scale. In many fields, including medical and materials research, the semiconductor industry, and forensic-science laboratories, scanning electron microscopes (SEM) and transmission electron microscopes (TEM) and are used. Both of SEM and TEM use a beam of electrons directed at the specimen for produce and magnified image of the sample. And also lots of features, such as electron gun, condenser lenses and vacuum system,which are similar in both instruments. But the main differences between them is SEM primarily used to study the surface, or near surface structure of bulk specimens, whereas TEM is gives information about the internal structure of thin specimens. The principle of a scanning electron microscope is shown schematically in Figure 3.10.

The scanning electron microscope comprises of two main parts: an electron column, and an electron detector. The electron column of a SEM with a thermionic source contains the following components:

- Filament (the cathode) – used as a electron source of the SEM
- Wehnelt Cylinder – (i) focuses the electron beam
  (ii) stabilizes the beam current.
- Anode Plate - accelerates the free electrons down the column with preserve the high voltage difference between the anode and the cathode,
- Condenser Lens – control the diameter of the electron beam, it primarily used to reduce the diameter of the beam to produce a smaller spot size.

- Scan Coils - electromagnetically raster the electron beam on the specimen surface.
- Final Objective Lens - focuses the electron beam on the surface of the specimen. The smallest spot is about 5 nm (down to 1nm with a field emission source).
- Detectors

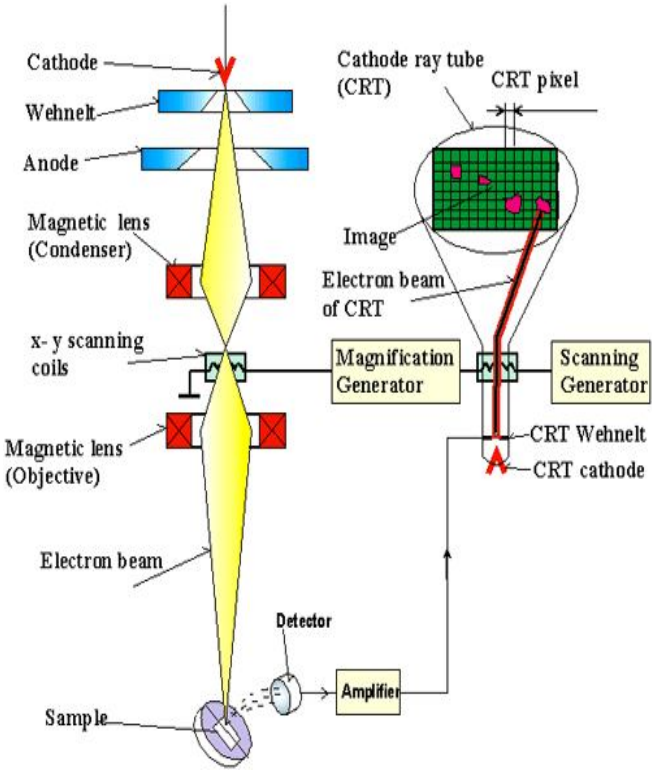

Figure 3.10 : Schematic illustration of scanning electron microscope (SEM) (adapted from Url-3)

Interaction between the incoming electron and an atomic nucleus can be classified in two different types, namely elastic and inelastic interactions. In elastic scattering electrons does not transfer their energy but in inelastic scattering process, the incoming fast electrons lose its appreciable amount of energy. The energy transferred to the specimen can cause different signals such as X-rays, Auger or secondary electrons, plasmons, phonons, UV quanta which give information about the topography, the electronic structure, and the composition of the specimen. Figure 3.11 demonstrate the schematic view of the electron-matter interactions arising from the impact of the electron beam onto a sample.

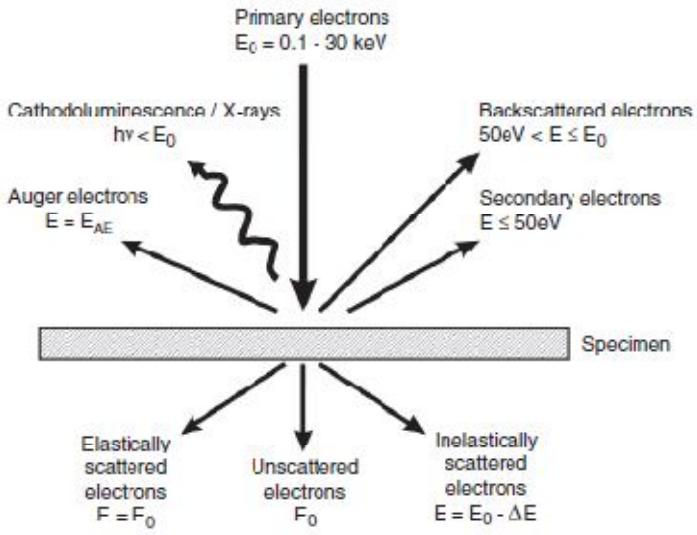

Figure 3.11 : Scheme of electron-matter interactions arising from the impact of an electron beam onto a specimen (Egerton, 2005)

Incoming electrons can be reflected (backscattered) from a bulk sample or can give their energy to atomic electron of the sample which generates the secondary electrons by release of atomic electron from the nucleus. The secondary electron coefficient (δ) is change slightly with atomic number whereas the backscattered electron coefficient (η) increases with increasing atomic number of the specimen. Due to the low energy of the secondary electron, in the energy range of 50eV, these electrons have only a few nanometer escape depth from the surface. In the SEM technique, the information about the surface is coming from the distance between 1 nm and10 nm. Therefore, the signals of the secondary electrons can be utilized for image formation in the SEM. A backscattered electron is a primary electron that has been ejected from the sample with a angle which is greater than 90 degrees and the energy of the backscattered electron in the range of 50 eV < $E_{BSE} \leq E_0$. On the basis of their kinetic energy the secondary electron and the backscattered electrons can be distinguish. Another main differences between the images which obtain from the back scattered electron signals and the secondary electron signals, is the depth from which the information originates. In the back scattered image, the signals comes from a depth of up to about half the penetration depth. Backscattered electron images can show contrast due to variations in chemical composition of a specimen, whereas the secondary electron images demonstrate mainly its surface topography.

4. EXPERIMENTAL PROCEDURE

Present study investigates the thermal properties and crystal structure of binary GeO_2 – V_2O_5 glass system doped with erbium and in undoped conditions. There is no data available on the crystallization kinetics, microstructural morphology and thermal properties on this glass system. Therefore this research is intended to fulfill the task of completing this incomplete knowledge.

4.1 Glass Synthesis

Nine different glass compositions (in moles) which are 0.70 GeO_2 – 0.30 V_2O_5 , 0.58 GeO_2 – 0.42 V_2O_5 , 0.40 GeO_2 – 0.60 V_2O_5, 0.695 GeO_2 – 0.30 V_2O_5 – 0.005 Er_2O_3, 0.575 GeO_2 – 0.42 V_2O_5 – 0.005 Er_2O_3, 0.40 GeO_2 – 0.595 V_2O_5 – 0.005 Er_2O_3 , 0.69 GeO_2 – 0.30 V_2O_5 – 0.01 Er_2O_3 , 0.57 GeO_2 – 0.42 V_2O_5 – 0.01 Er_2O_3, 0.40 GeO_2 – 0.59 V_2O_5 – 0.01 Er_2O_3 were obtained by reagent grade of GeO_2 (99,99% purity, Aldrich), V_2O_5 (99,5% purity, Aldrich) and Er_2O_3 (99,99% purity, Aldrich) powders. Powder batches of glass compositions are given in Table 4.1 and the batches of 4g in size which were prepared by weighing in Precisa^{TM} XB220A sensitive balance and mixed throughly for 15 minutes to have homogenous powders. Mixed raw materials were heated in a platinum crucible to 900°C with 20°C/min heating rate in an electrically heated furnace. The resultant mixture were removed from furnace and quenched immediately by dipping the crucible in a shallow water bath. Glass melting experiments and annealing process were carried out by using a Protherm™ furnace shown in Figure 4.1.

Figure 4.1 : Protherm™ furnace.

Table 4.1: Compositions in mole amounts and in weight amounts (grams) of the GeO_2, V_2O_5 and Er_2O_3

Compositions (mol)	**GeO_2 (grams)**	**V_2O_5 (grams)**	**Er_2O_3 (grams)**
0.70 GeO_2 – 0.30 V_2O_5	2.2921	1.707	0
0.58 GeO_2 – 0.42 V_2O_5	1.7707	2.229	0
0.40 GeO_2 – 0.60 V_2O_5	1.1086	2.891	0
0.695 GeO2 – 0.3 V2O5 – 0.005 Er2O3	2.2512	1.6896	0.0592
0.575 GeO2 – 0.42 V2O5 – 0.005 Er2O3	1.7378	2.2070	0.0553
0.40 GeO2 – 0.595 V2O5 – 0.005 Er2O3	1.1013	2.8483	0.0503
0.69 GeO2 – 0.3 V2O5 – 0.01 Er2O3	2.2112	1.6716	0.1172
0.57 GeO2 – 0.42 V2O5 – 0.01 Er2O3	1.7056	2.1850	0.1094
0.40 GeO2 – 0.59 V2O5 – 0.01 Er2O3	1.0941	2.8059	0.1000

The composition of the vanadium germanate glass was chosen from a journal which focuses on phase diagram of vanadium germanate binary glass system (Marinov et al.,1975). Figure 4.2 reveals the phase diagram of the binary vanadium germanate glass. Regarding this phase diagram, three composition of the glass were chosen as one hypereutectic (60 mol% V_2O_5 content), one hypoeutectic(30 mol% V_2O_5 content) and one eutectic (42 mol% V_2O_5 content) compositions.

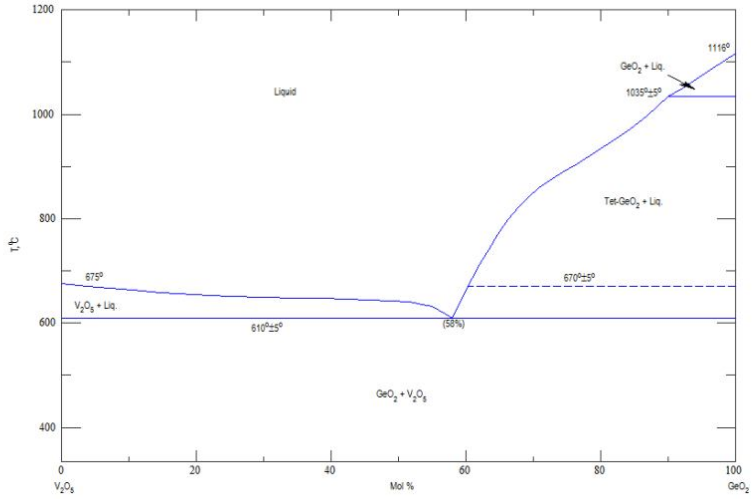

Figure 4.2: Phase-equilibrium in GeO_2-V_2O_5 system(Marinov et al.,1975)

3.2 Thermal Characterizations

To observe thermal behavior of as-cast samples, differential thermal analysis (DTA) experiments were carried out in a TA^{TM} Q600 DTA/TGA/DSC (Figure 4.3) on binary GeO_2-V_2O_5 glass compositions of the present study.

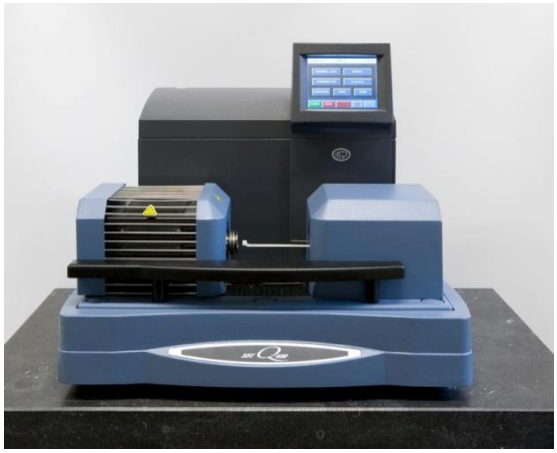

Figure 4.3 : TA™ Instruments Q600 DTA/TGA/DSC.

After pulverizing and grinding as-cast glass, DTA experiments were performed by heating powdered glass samples between 50°C to 900°C and 50°C to 1100°C at heating rates of 5.10.15 and 20°C/min in aplatinum crucible in which alumina powder was used as a reference material in DTA.

Glass transition temperature (T_g) ,crystallization peak temperature (T_p) and melting temperatures(T_m) were determined by using TA Instrument Universal Analysis Program™.

4.3 Microstructural Characterizations

4.3.1 X-ray diffraction (XRD) characterizations

In order to understand the formation or transformation of the crystalline phases that may exist in the Er_2O_3 doped and non-doped GeO_2-V_2O_5 binary glass systems, X-ray diffractometry scans were conducted on the heat-treated glass samples. On the basis of DTA investigation the glasses annealed above the respective peak temperatures followed by quenching in water. The X-ray diffraction investigations were carried out in a Bruker™ D8 Advanced Series powder diffractometer shown in Figure 3.4 by using Cu Kα radiation at 40 kV and 40 mV settings in the 2θ□ range from 10° to 90° with step size 0.02.

All samples were ground to powder for XRD scans and the crystallized phases were identified by comparing the peak positions and intensities with those in the JCPDS (Joint Committee on Powder Diffraction Standards) data files.

Figure 4.4 : Bruker™ D8 Advanced Series powder diffractometer.

4.3.2 Scanning electron microscope (SEM) characterizations

Scanning Electron Microscope (SEM) investigations were performed on heat-treated samples in a JEOL™ JSM 5410 which is shown in Figure 4.5 operated at 15kV and linked with Noran™ 2100 Freedom energy dispersive spectrometer (EDS) attachment and in a JEOL JSM 7000F Field Emission Scanning Electron Microscope which is shown in Figure 4.6. Samples were etched in a %80 distilled water + %20 H.F acid solution for 3-5 seconds and etched samples were coated with palladium-gold for the SEM and EDS operations.

Figure 4.5 : JEOL^{TM} JSM 5410 scanning electron microscope.

Figure 4.6 : JEOL JSM 7000F Field Emission Scanning Electron Microscope.

5. RESULTS AND DISCUSSION

5.1 0.70 GeO_2 - 0.30 V_2O_5 Glass

As-cast 0.70 GeO_2 – 0.30 V_2O_5 glass samples are shown in Figure 5.1. As seen in Figure 5.1, as-cast 0.70 GeO_2 – 0.30 V_2O_5 glass samples have black color under visible light.

Figure 5.1 : As-cast 0.70 GeO_2 – 0.30 V_2O_5 glass samples

5.1.1 DTA investigations of the 0.70 GeO_2 - 0.30 V_2O_5 glass

DTA investigation was conducted on the as-cast 0.70 GeO_2 – 0.30 V_2O_5 glass samples to understand the thermal properties. DTA thermograph of the glass specimen scanned between 50 and 900°C with 10 °C/min heating rate is given in Figure 5.2.

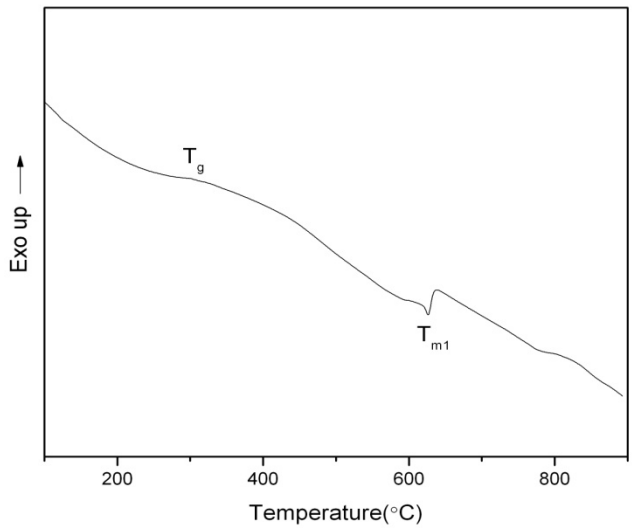

Figure 5.2 : DTA scans of the as-cast non-doped 0.70 GeO_2 - 0.30 V_2O_5 glass with the heating rate of 10 °C/min.

DTA curves show typical nature of a glass with a small broad endothermic peak corresponding to the glass transition temperature (T_g) and the endothermic melting peak (T_m) temperature. Characteristic temperatures of the 0.70 GeO_2 - 0.30 V_2O_5 glass are presented in Table 5.1. Glass transition temperature (T_g) is 308°C and the melting temperature (T_m) is 624°C and there is no detectable exothermic peak on the DTA curve which indicates that these binary glass system has great stability against the crystallization.

Table 5.1 : Characteristic temperatures of the 0.70 GeO_2 - 0.30 V_2O_5 glass.

	0.70 GeO_2 - 0.30 V_2O_5			
T (°C)	T_g	T_x	T_{p1}	T_m
10 °C/min	308.05	-	-	624.88

In order to determine the annealing temperature, a new DTA curve was plotted using the derivative of the DTA curve belonging to the as-cast 0.70 GeO_2 - 0.30 V_2O_5 glass. Figure 5.3 shows the derivative DTA curves of the 07 GeO_2 – 0.30 V_2O_5 glass with 10°C/min heating rates. Even though there is no observable exothermic peak on the DTA curve, a slight change of slope is observed at 446°C on the DTA curve which is plotted using the derivative over temperature. Thus, the annealing temperature is chosen as 500°C , which is higher than this bend.

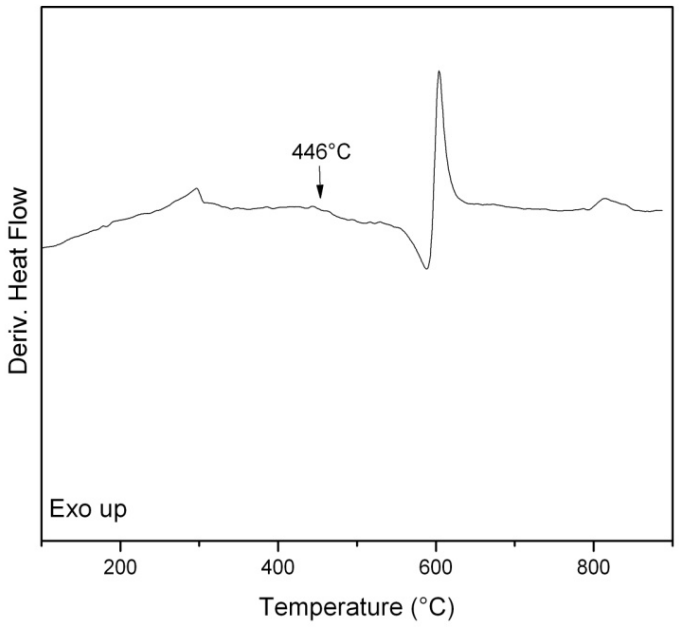

Figure 5.3 : Derivative DTA curves of the 07 GeO_2 – 0.30 V_2O_5 glass with 10°C/min heating rates

5.2.2 XRD analysis of the 0.70 GeO_2 - 0.30 V_2O_5 glass

On the basis of DTA results, XRD investigation were carried out to identify the crystallizing phases in the glassy matrix. Figure 5.4 are the XRD patterns of 0.70 GeO_2 - 0.30 V_2O_5 glass in the as-cast and the same after heat treatment. Glass samples demonstrate amorphous structure in the as-cast condition as seen in Figure 5.4(a). The heat treated glass samples were prepared by heating the as-cast glasses to 500°C for 2 hours with 10°C/min heating rates, followed by quenching in water.

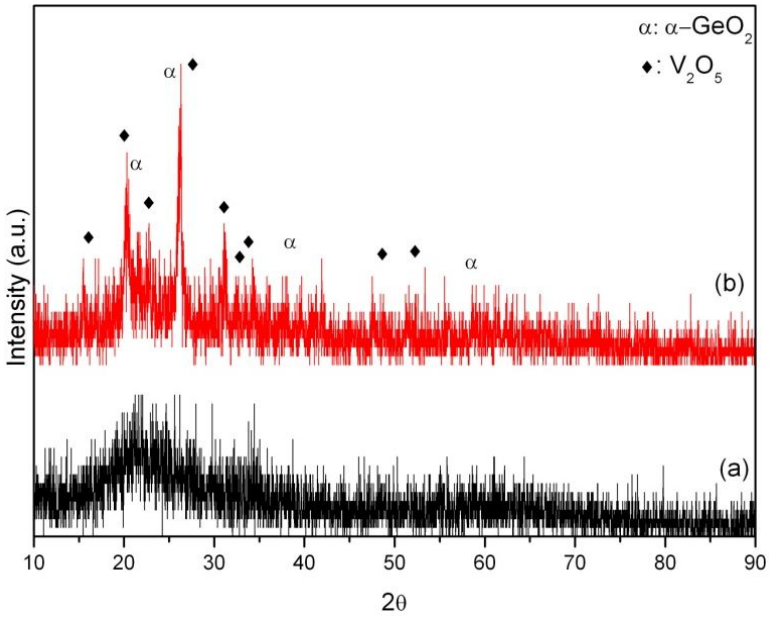

Figure 5.4 : XRD scans of the 0.70 GeO_2 – 0.30 V_2O_5 glasses which are as-cast (a) and annealed at 500 °C (b)

The XRD pattern of the heat treated 0.70 GeO_2 – 0.30 V_2O_5 glass reveal the presence of a hexagonal GeO_2 phase and an orthorhombic V_2O_5 crystalline phase. The structures of the crystals, lattice parameters, space groups and card numbers of the crystalline phases, observed in the glasses are given in Table B 1.

5.2.3 SEM investigations of the 0.70 GeO_2 - 0.30 V_2O_5 glass

In order to understand the morphology of the resultant microstructures after crystallization, SEM/SEI analyses were carried out on the binary GeO_2 - V_2O_5 glass with 30 mol % V_2O_5 content. Glass specimens were quenched in water right after annealed at 500°C for 2 hours with 10°C/min heating rate. The SEM/SEI micrographs were taken from cross-section of heat treated and etched 0.70 GeO_2-0.30 V_2O_5 glass samples.

Figure 5.5 shows the morphology of the glass structure after annealing at 500°C. The structure reveals presence of sphere-shaped crystals varying between 0.34µm to 0.50µ in size and grape like crystal on the average of 2 µm in size.

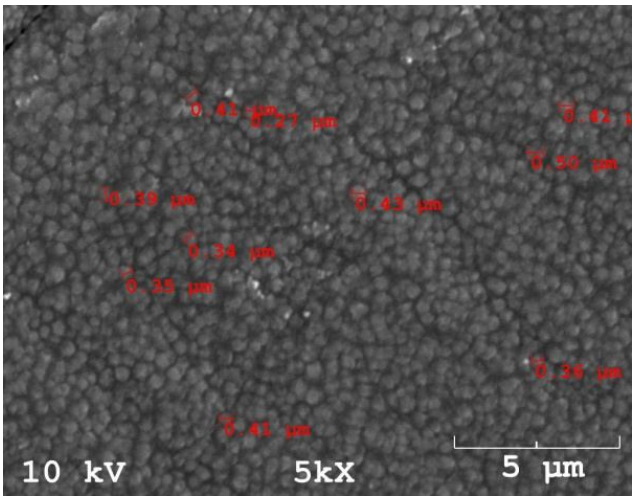

(a)

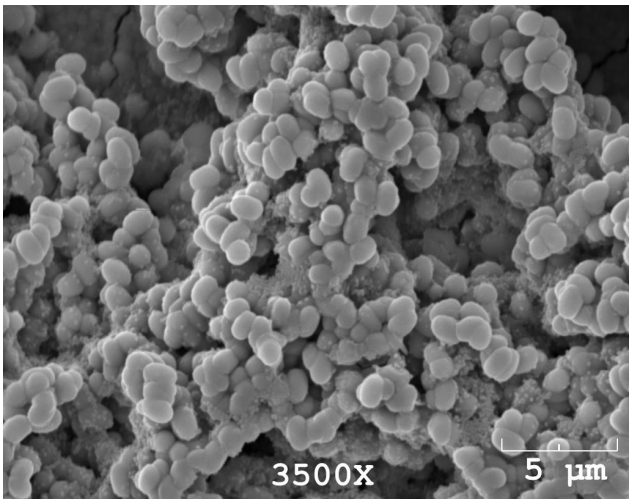

(b)

Figure 5.5 : SEM micrographs of the crystalline regions of the non-doped 0.70 GeO_2 – 0.30 V_2O_5 glass samples which was heat treated at 500 °C: (a) 5000x, (b) 3500x.

EDS analyses were performed on the crystalline regions which is shown in Figure 5.5(a), revealed that (10.87 wt% Ge, 69.87 wt% O, 19.253 wt% V) sphere-shaped structure consists of vanadium rich crystals. And when the EDS measurements were taken from the crystalline regions of grape-like structure in Figure 5.5 (b), it shows that these structures are germanium rich structure. Regarding to the XRD results, it is obvious that sphere shaped structures belongs to V_2O_5 crystal and grape-like structures belongs to hexagonal form of GeO_2 crystal (α-GeO_2).

5.2 0.58 GeO_2 - 0.42 V_2O_5 Glass

As-cast 0.58 GeO_2 – 0.42 V_2O_5 glass samples are shown in Figure 5.6. As seen in Figure 5.6, as-cast 0.58 GeO_2 – 0.42 V_2O_5 glass samples have black color under visible light.

Figure 5.6 : As-cast 0.58 GeO_2 – 0.42 V_2O_5 glass samples

5.2.1 DTA investigations of the 0.58 GeO_2 - 0.42 V_2O_5 glass

DTA thermal investigations were conducted on the as-cast 0.58 GeO_2 - 0.42 V_2O_5 glass sample. The samples were heated to 900°C with different heating rate of 10°C/min as seen in Figure 5.7.

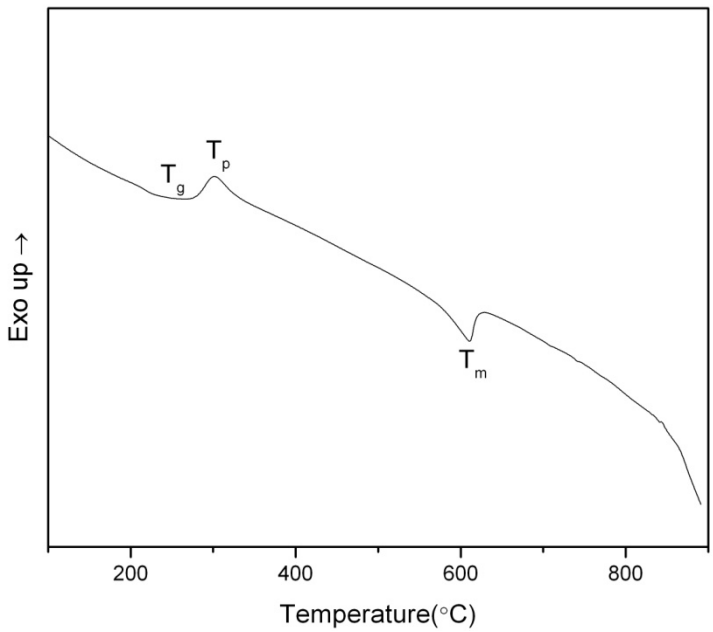

Figure 5.7 : DTA scans of the as-cast non-doped 0.58 GeO_2 - 0.42 V_2O_5 glass with the heating rate of 10 °C/min

DTA thermogram of 0.58 GeO_2 - 0.42 V_2O_5 glass samples revealed that one exothermic peak which means that distinct from the 0.70 GeO_2 - 0.30 V_2O_5 glass

samples, crystallization mechanism occur for this composition. After exothermic peak, one endothermic peak follows which demonstrate the melting of the crystalline phases in the glass samples.

Characteristic temperatures and on-set crystallization temperatures (T_x) are given in Table 5.2.

Table 5.2 : Characteristic temperatures of the 0.58 GeO_2 – 0.42 V_2O_5 glass.

	0.58 GeO_2 – 0.42 V_2O_5			
T (°C)	T_g	T_x	T_{p1}	T_m
10 °C/min	218.85	278.97	301.5	610.69

Glass transition temperatures (T_g) lays at 218ºC while the melting temperatures (T_m) exist at 610 ºC and the crystallization peak temperatures (T_p) present at 301°C

5.2.2 XRD analysis of the 0.58 GeO_2 - 0.42 V_2O_5 glass

On the basis of XRD pattern shown in Figure 5.8(a), binary GeO_2 – V_2O_5 glass containing 42 mol% V_2O_5 has an amorphous structure in the as-cast condition.

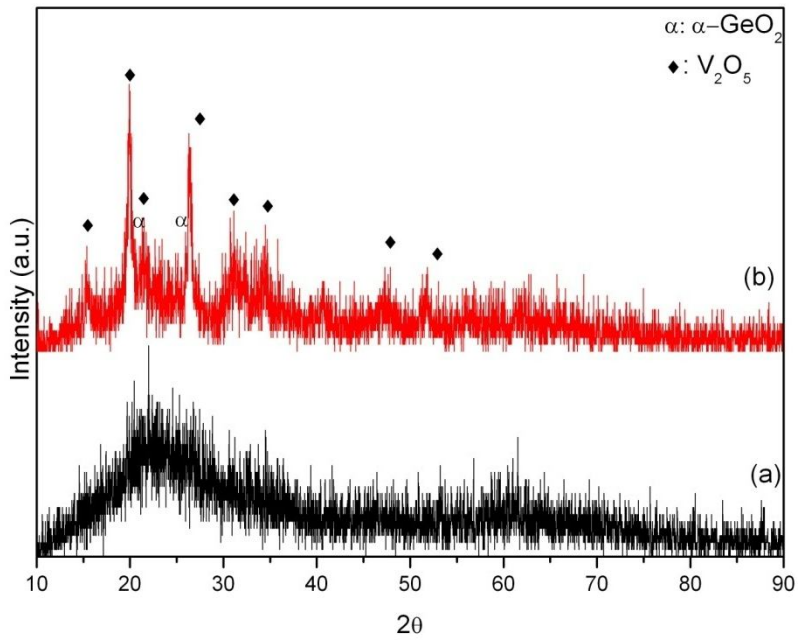

Figure 5.8 : XRD scans of the 0.58 GeO_2 – 0.42 V_2O_5 glasses which are as-cast (a) and annealed at 400 °C (b)

Figure 5.8(b) show the X-ray diffraction patterns taken from the 0.58 GeO_2 - 0.42 V_2O_5 glass samples which heated to 400°C (above the peak crystallization temperature) at a rate of 10°C/min followed by water quench. As seen from the Figure 5.8(b) orthorhombic V_2O_5 crystals are the dominant phase in the pattern while

the α-GeO_2 crystalline phase exhibits only two crystal peaks. It can be deduced that the α-GeO_2 has crystallized in small quantities while the V_2O_5 crystals show wide-spread crystallization in the glass matrix.

The structures of the crystals, lattice parameters, space groups and card numbers of the crystalline phases observed in the glasses are given in Table B.1.

5.2.3 SEM investigations of the 0.58 GeO_2 - 0.42 V_2O_5 glass

After identifying the crystalline phase with XRD analysis, SEM investigations were performed to understand the morphology of the consequent microstructures after annealing. SEM/SEI micrographs were taken from the surface of the 0.58 GeO_2 – 0.42 V_2O_5 glass samples which were annealed at 400 °C for 2h with a heating rate of 10 °C/min followed by quenching in water.

Figure 5.9 (a) and (b) are representative the SEM/SEI micrographs taken from the cross section of the 0.58 GeO_2- 0.42 V_2O_5 glass which consist of vanadium rich crystals. Colony formation of V_2O_5 crystals which reside in the surface of the sample can be observed from Figures 5.9 (a) and (b). EDS analyses performed on these colonies (6.437 wt% Ge, 70.509 wt% O, 23.053 wt% V) revealed that these crystalline regions belong to V_2O_5 crystals. Therefore, it can be stated that that the sphere shaped V_2O_5 crystals which is seen in Figure 5.5 (a), were transformed to the colony structure of V_2O_5 crystals in 0.58 GeO_2- 0.42 V_2O_5 glass with increasing content of V_2O_5.

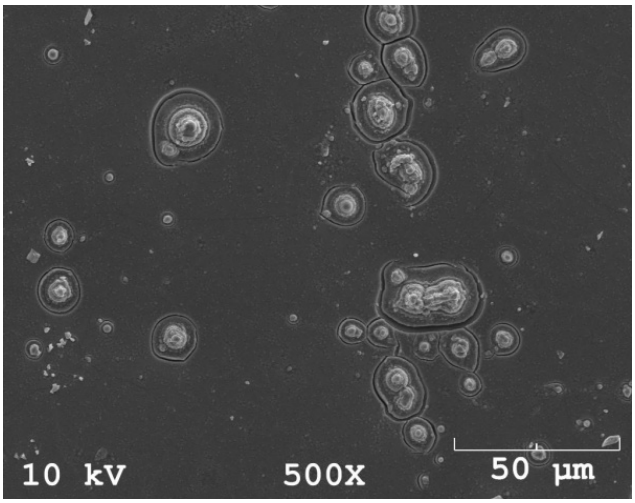

(a)

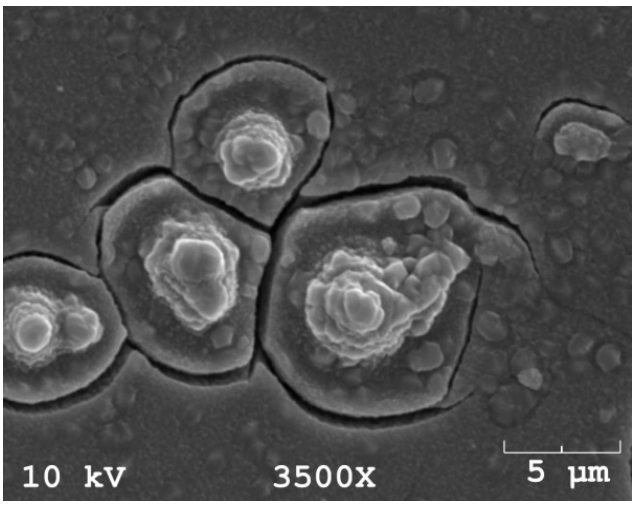

(b)

Figure 5.9 : SEM micrographs of the crystalline regions of the undoped 0.58 GeO_2 – 0.42 V_2O_5 glass samples which was heat treated at 400 °C: (a) 500x, 3500x (b)

V_2O_5 nano-cracks which are seen in in Figure 5.9 (a) and (b), are believed to be due to the differences of thermal expansion coefficients of the V_2O_5 and the glass matrix.

5.3 0.40 GeO_2 - 0.60 V_2O_5 Glass

As-cast 0.40 GeO_2 – 0.60 V_2O_5 glass samples are shown in Figure 5.10. As seen in Figure 5.10, as-cast 0.40 GeO_2 – 0.60 V_2O_5 glass samples have black color under visible light.

Figure 5.10: As-cast 0.40 GeO_2 – 0.60 V_2O_5 glass samples

5.3.1 DTA investigations of the 0.40 GeO_2 - 0.60 V_2O_5 glass

DTA curve for the as cast 0.40 GeO_2 – 0.60 V_2O_5 glass with the heating rate of 10 °C/min is demonstrated in Figure 5.11.

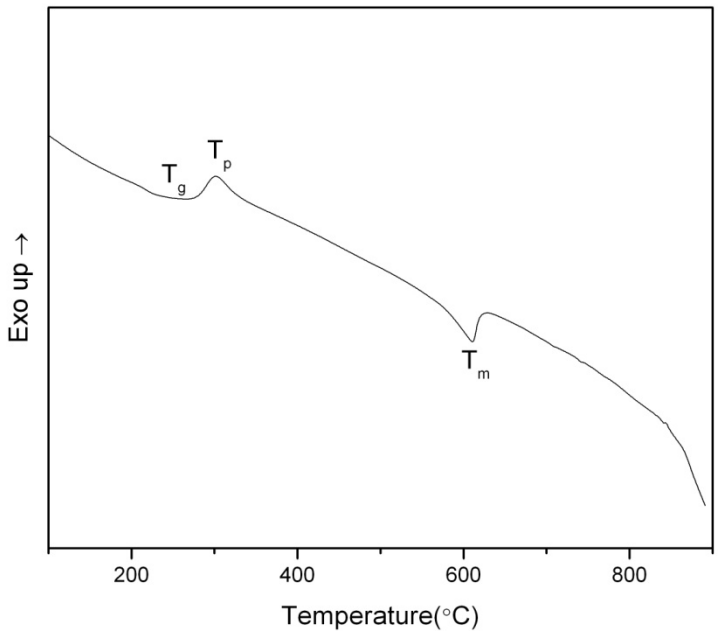

Figure 5.11 : DTA scans of the as-cast non-doped 0.40 GeO_2 - 0.60 V_2O_5 glass with the heating rate of 10 °C/min

As seen in DTA curves of the 0.40 GeO_2 - 0.60 V_2O_5 glasses, there is only one exothermic peak is present for the thermally treated glass samples which are very close to the glass transition temperature therefore, it can be statetd that the crystallization stability of the glass is too low. After exothermic peak, one endothermic peak is demonstrated on the curve.

Characteristic temperatures and on-set crystallization temperatures (T_x) are given in Table 5.3. Glass transition temperature (T_g) lays at 209 ºC while crystallization peak temperatures (T_p) exist at 242 º and the melting temperatures (T_m) present at 630 °C.

Table 5.3 : Characteristic temperatures of the 0.40 GeO_2 - 0.60 V_2O_5 glass.

	0.40 GeO_2 - 0.60 V_2O_5			
T (°C)	T_g	T_x	T_{p1}	T_m
10 °C/min	209.13	236.87	242.67	630.69

5.3.2 XRD analysis of the 0.40 GeO_2 - 0.60 V_2O_5 glass

X-ray diffractometry scans were carried out on the basis of DTA results to identify the crystalline phases in the glasses which were annealed above the respective peak temperatures. Binary GeO_2-V_2O_5 non-doped glass with 60 mol % V_2O_5 content demonstrate amorphous structure in the as-cast condition as seem in Figure 5.12(a).

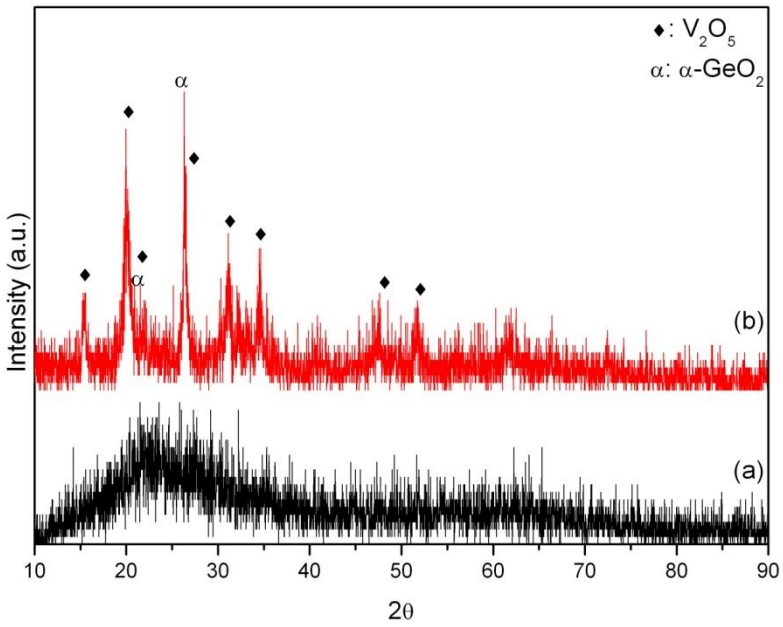

Figure 5.12 : XRD scans of the 0.40 GeO_2 – 0.60 V_2O_5 glasses which are as-cast (a) and annealed at 400 °C (b).

Figure 5.12(b) represents that XRD pattern of heat treated glass samples which were prepared by heated to 400°C for 2 hours with 10°C/min heating rate, followed by water quench. XRD pattern of annealed 0.4 GeO_2 – 0.6 V_2O_5 glass sample indicated the presence of small amount of hexagonal GeO_2 phase in addition to high amount of orthorhombic V_2O_5 crystalline phase. The structures of the crystals, lattice parameters, space groups and card numbers of the crystalline phases observed in the glasses are given in Table B.1

5.3.3 SEM investigations of the 0.40 GeO_2 - 0.60 V_2O_5 glass

To obtain better understanding of the morphology and size of the crystalline phases, SEM/SEI investigation were carried out to 0.40GeO_2- 0.60 V_2O_5 annealed glass

samples. Figure 5.13 (a) and (b) shows a series of SEM micrographs taken from the surface of samples which were heated to 400°C for 2h with a heating rate of 10°C/min followed by quenching in water.

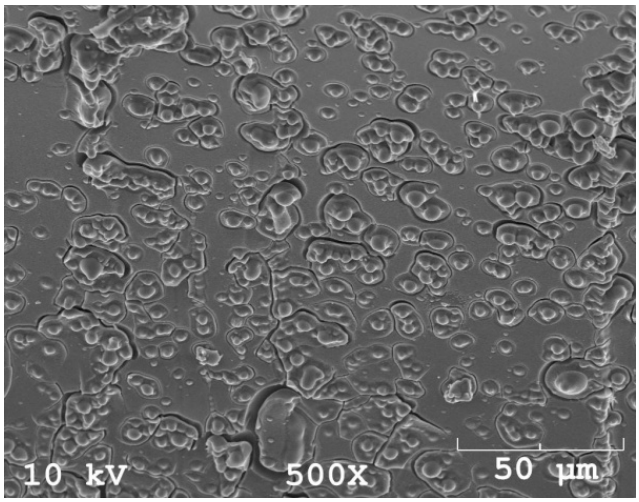

(a)

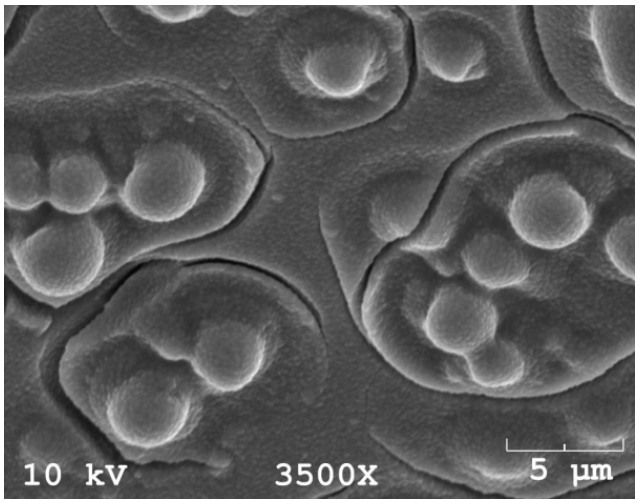

(b)

Figure 5.13 : SEM micrographs of the crystalline regions of the undoped 0.40 GeO_2 – 0.60 V_2O_5 glass samples which was heat treated at 400 °C: (a) 500x, (b) 3500x

Figure 5.13 reveal the presence of large globular-like orthorhombic V_2O_5 crystal on the average of 5µm in size. When the Figure 5.13(b) were observed more closely it can be seen that crystalline structure consists of little sphere like crystals. EDS measurements which were taken from the crystalline regions of the annealed glass samples revealed (13.79 wt% Ge, 8,779 wt% O, 77.421 wt% V) that these crystalline structures consist of vanadium rich structures. On the basis of the XRD results, the structure can be identified as a V_2O_5 crystalline phase. Like 0.42 GeO_2- 0.58 V_2O_5

glass samples, thermal expansion difference between the crystalline phase and glass matrix, causes the nano-cracks which were surrounding to the crystalline phase.

5.4 0.695 GeO_2 – 0.30 V_2O_5 – 0.005 Er_2O_3 Glass

As-cast 0.695 GeO_2 – 0.30 V_2O_5 – 0.005 Er_2O_3 glass samples are shown in Figure 5.14. As seen in Figure 5.14, as-cast 0.695 GeO_2 – 0.30 V_2O_5 – 0.005 Er_2O_3 glass samples have black color under visible light.

Figure 5.14 : As-cast 0.695 GeO_2 – 0.30 V_2O_5 – 0.005 Er_2O_3 glass samples

5.4.1 DTA investigations of the 0.695 GeO_2 – 0.30 V_2O_5 – 0.005 Er_2O_3 glass

DTA thermogram of as-cast 0.695 GeO_2 – 0.30 V_2O_5 – 0.005 Er_2O_3 glass sample heated to 900°C with heating rates 10 °C/min, are demonstrated in Figure 5.15. DTA curves show typical nature of a glass with a small broad endothermic peak corresponding to the glass transition temperature (T_g) and the endothermic melting peak (T_m) temperature.

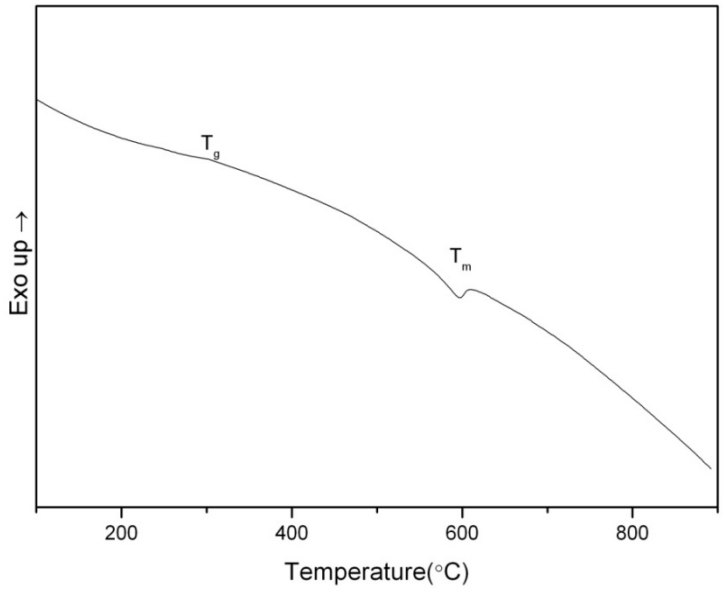

Figure 5.15 : DTA scan of the as-cast doped 0.695 GeO_2 – 0.30 V_2O_5 – 0.005 Er_2O_3 glass with the heating rate of 10 °C/min.

Characteristic temperatures of the 0.695 GeO_2 – 0.30 V_2O_5 – 0.005 Er_2O_3 glass are presented in Table 5.4. Glass transition temperature (T_g) is 304°C and the melting temperature (T_m) is 595°C and there is no detectable exothermic peak on the DTA curves like the 30 mol% V_2O_5 containing non-doped binary glass samples which indicate that these binary glass systems have great stability against the crystallization.

Table 5.4 : Characteristic temperatures of the 0.695 GeO_2 - 0.30 V_2O_5 -0.005 Er_2O_3 glass

0.695 GeO_2 – 0.30 V_2O_5– 0.005 Er_2O_3				
T (°C)	T_g	T_x	T_{p1}	T_m
10 °C/min	304.05	-	-	595.88

5.4.2 XRD analysis of the 0.695 GeO_2 – 0.30 V_2O_5 – 0.005 Er_2O_3 glass

XRD investigations were carried out to investigate crystalline phases of the 0.695 GeO_2 – 0.30 V_2O_5 – 0.005 Er_2O_3 glasses. The heat treated glass samples were prepared by water quenching right after heating the as-cast glass samples to 700°C for 2 hours with a 10°C/min.

Figure 5.16 shows the XRD pattern of 0.695 GeO_2 – 0.30 V_2O_5 – 0.005 Er_2O_3 glasses in the as-cast condition and after annealing at 700°C. As seen in Figure 5.16(a), some low intensity peaks which belong to $ErVO_4$ crystals, existed for the 0.695 GeO_2 – 0.30 V_2O_5 – 0.005 Er_2O_3 glasses in the as-cast condition.

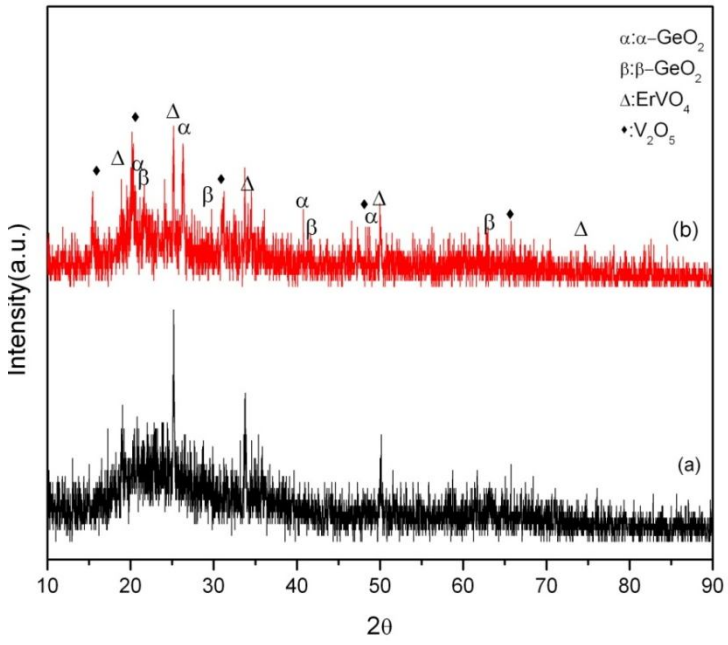

Figure 5.16 : XRD scans of the 0.695 GeO_2 – 0.30 V_2O_5– 0.005 Er_2O_3 glasses which are as-cast (a) and annealed at 500 °C (b)

XRD patterns of annealed glass were revealed the presence of tetragonal β-GeO_2, hexagonal α-GeO_2, orthorhombic V_2O_5 and tetragonal $ErVO_4$ crystalline phases in its structure. The structures of the crystals, lattice parameters, space groups and card numbers of the crystalline phases observed in the glasses are given in Table B.1.

5.4.3 SEM investigations of the 0.695 GeO_2 – 0.30 V_2O_5 – 0.005 Er_2O_3 glass

SEM/SEI investigations were performed on the 0.695 GeO_2 – 0.30 V_2O_5 – 0.005 Er_2O_3 glasses in order to identify and analyze the morphology and size of the crystallizing phases. Figure 5.17(a)–(b) shows a series of SEM micrographs taken from glass samples heated to 500 ◦C followed by quenching in water.

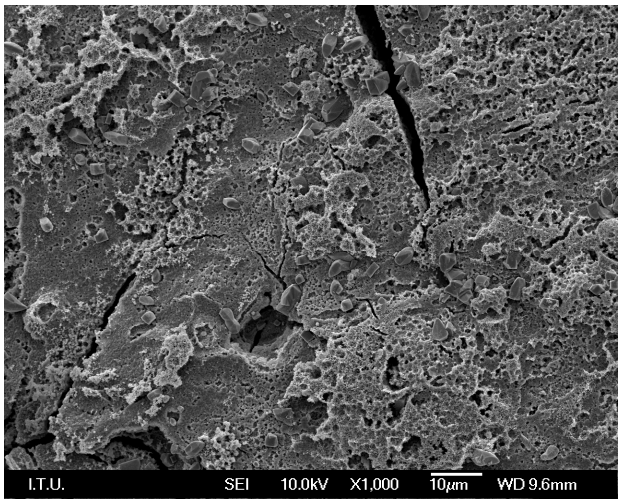

(a)

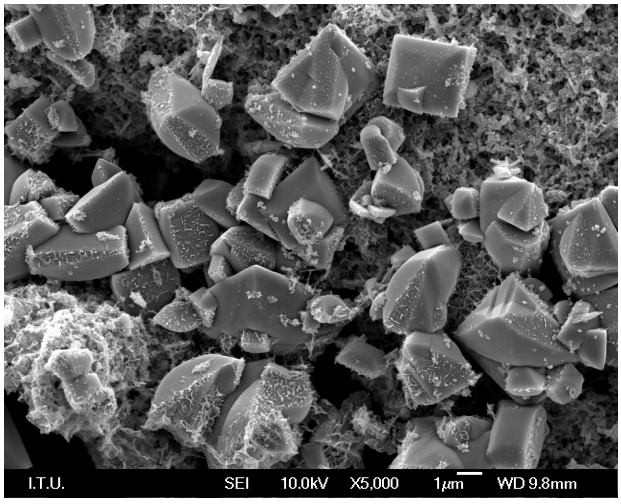

(b)

Figure 5.17 : SEM micrographs of the crystalline regions of the 0.695 GeO_2 – 0.10 V_2O_5 – 0.005 Er_2O_3 glass samples which was heat treated at 700 °C: (a) 1000x, (b) 5000x.

Even though there are four kind of crystalline phase were observed in the XRD pattern of the samples, SEM/SEI micrographs reveal the presence of only one kind of morphology, varying between 3μ m and 5μm in size. EDS spectra taken from these regions have shown that they contained 38.21 wt% Ge, 54.82 wt% O, 6.97 wt% V indicating that this crystalline region GeO_2-rich regions (i. e. Containing α-GeO_2 and/or β-GeO_2 phases).

5.5 0.575 GeO_2 – 0.42 V_2O_5 – 0.005 Er_2O_3 Glass

As-cast 0.575 GeO_2 – 0.42 V_2O_5 – 0.005 Er_2O_3 glass samples are shown in Figure 5.18. As seen in Figure 5.18, as-cast 0.575 GeO_2 – 0.42 V_2O_5 – 0.005 Er_2O_3 glass samples have black color under visible light.

Figure 5.18 : As-cast 0.575 GeO_2 – 0.42 V_2O_5 – 0.005 Er_2O_3 glass samples

5.5.1 DTA investigations of the 0.575 GeO_2 – 0.42 V_2O_5 – 0.005 Er_2O_3 glass

Differential thermal (DTA) investigations were conducted on the as-cast 0.575 GeO_2 – 0.42 V_2O_5 – 0.005 Er_2O_3 glasses. Figure 5.19 shows the respective DTA data of the as-cast glass samples scanned at a rate of 10°C/min between 100 and 900°C.

As seen in Figure 5.19, the DTA scans exhibit small endothermic peaks at 219°C as the glass transition temperature, T_g , and the melting temperatures (T_m) present at 612 °C. Crystallization processes taking place in the glass matrix are marked by exothermic peak (T_p) at 301°C, indicating that the crystallization mechanism occurred for the glass samples.

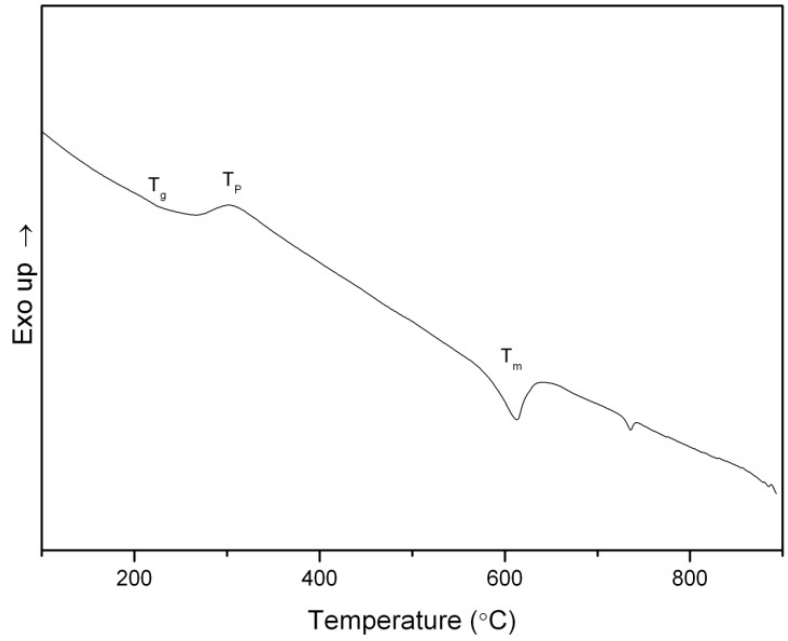

Figure 5.19: DTA scan of the as-cast doped 0.575 GeO_2 – 0.42 V_2O_3 – 0.005 Er_2O_3 glass with the heating rate of 10 °C/min.

Characteristic temperatures and on-set crystallization temperatures (T_x) are given in Table 5.5.

Table 5.5 : Characteristic temperatures of the 0.575 GeO_2 - 0.42 V_2O_5 -0.005 Er_2O_3 glass.

0.575 GeO_2 – 0.42 V_2O_5 – 0.005 Er_2O_3				
T (°C)	T_g	T_x	T_{p1}	T_m
10 °C/min	219.24	275.97	301.21	612.35

5.5.2 XRD analysis of the 0.575 GeO_2 – 0.42 V_2O_5 – 0.005 Er_2O_3 glass

In order to understand crystallization behavior, XRD investigations were conducted to 0.575 GeO_2 – 0.42 V_2O_5 – 0.005 Er_2O_3 glass systems.

Binary GeO_2-V_2O_5 glass doped with 0.5 mol % Er_2O_3 containing 42 mol% V_2O_5 shows amorphous structure in the as-cast condition as seem in Figure 5.20(a).

On the basis of DTA results, the samples were heated to 400°C for 2 hours with a 10°C/min heating rates, followed by quenching in water for annealing process. XRD pattern of annealed glass reveals the presence of the hexagonal α-GeO_2, orthorhombic V_2O_5 and little amount of tetragonal $ErVO_4$ and tetragonal Er_2O_3 crystalline phases in its structure

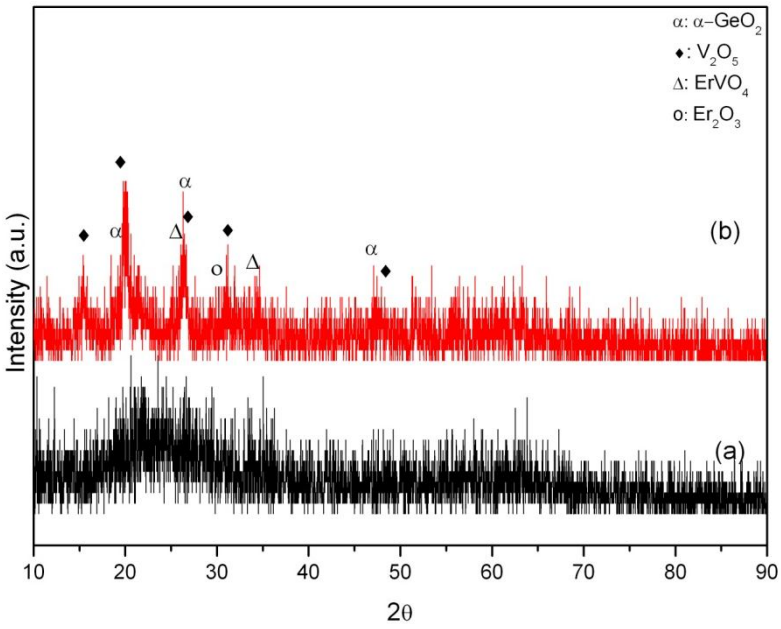

Figure 5.20 : XRD scans of the 0.575 GeO_2 – 0.42 V_2O_5– 0.005 Er_2O_3 glasses which are as-cast (a) and annealed at 400 °C (b)

The structures of the crystals, lattice parameters, space groups and card numbers of the crystalline phases observed in the glasses are given in Table B.1.

5.5.3 SEM investigations of the 0.575 GeO_2 – 0.42 V_2O_5 – 0.005 Er_2O_3 glass

In order to investigate morphology of the crystalline phases which are identified in the XRD investigations, SEM/SEI micrographs were taken from the surface of the doped 0.575 GeO_2 – 0.42 V_2O_5 – 0.005 Er_2O_3 glass-ceramic samples which were annealed at 700 °C for 2h with a heating rate of 10 °C/min and quenched in water afterwards. EDS measurements were taken from the crystalline regions.

Figure 5.21 (a) and (b) are representing the SEM/SEI micrographs that taken from the 0.575 GeO_2 – 0.42 V_2O_5 – 0.005 Er_2O_3 glass samples. The micrographs demonstrate two different types of crystalline phases which are spread to glassy matrix by nearly homogenous nucleation and bulk crystallization. Formation of the germanium rich crystals which mainly reside at surface of the sample can be seen as equaixed crystals in Figure 5.21 (a). In addition to these structures, formation of vanadium rich crystals is also observed as columnar-ball like crystals which is 60-80 nm in width and 200-600nm in length, in Figure 5.21(b). EDS analyses were performed on the crystalline regions (Figure 5.21(a)) and revealed that (24.47 wt% Ge, 9.75 wt% V, 65.79 wt% O) equiaxed crystals are Ge-rich crystals and can be belong to α-GeO_2 crystalline phase.

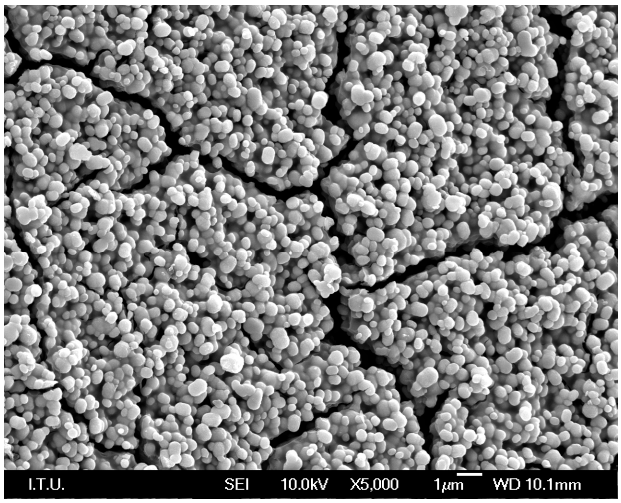

(a)

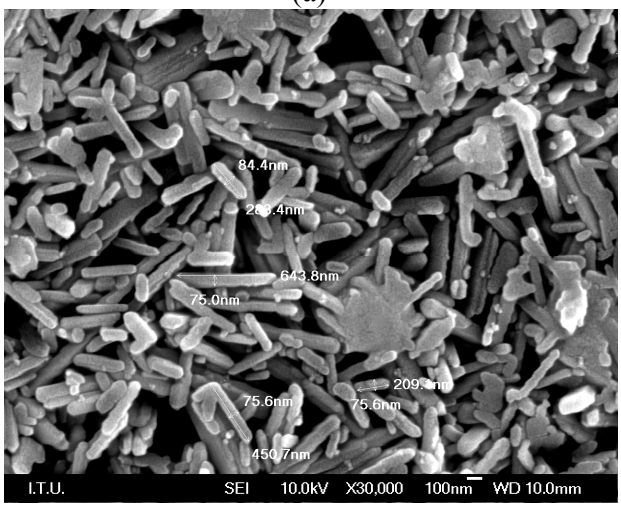

(b)

Figure 5.21 : SEM micrographs of the crystalline regions of the 0.575 GeO_2 – 0.42 V_2O_5 – 0.005 Er_2O_3 glass samples which was heat treated at 700 °C: (a) 5000x, (b) 30000x.

The columnar-ball like crystalline regions (Figure 5.21 (b)) indicate that (10.23 wt% Ge, 28.83 wt% V, 60.94 wt% O) these structures consist of V_2O_5 crystals.

5.6 0.40 GeO_2 – 0.595 V_2O_5 – 0.005 Er_2O_3 Glass

As-cast 0.40 GeO_2 – 0.595 V_2O_5 – 0.005 Er_2O_3 glass samples are shown in Figure 5.22. As seen in Figure 5.22, as-cast 0.40 GeO_2 – 0.595 V_2O_5 – 0.005 Er_2O_3 glass samples have black color under visible light.

Figure 5.22 : As-cast 0.40 GeO_2 – 0.595 V_2O_5 – 0.005 Er_2O_3 glass samples

5.6.1 DTA investigations of the 0.40 GeO_2 – 0.595 V_2O_5 – 0.005 Er_2O_3 glass

DTA curve for the as cast 0.40 GeO_2 – 0.595 V_2O_5 – 0.005 Er_2O_3 glass with the heating rate of 10 °C/min is demonstrated in Figure 5.23

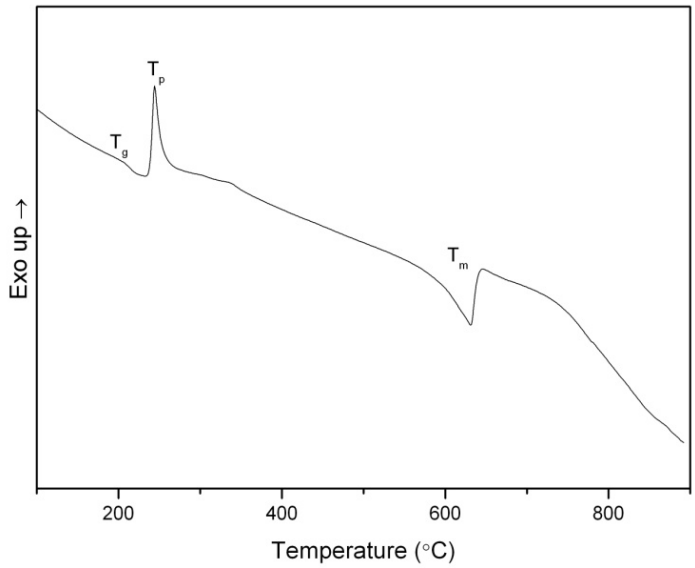

Figure 5.23 : DTA scan of the as-cast doped 0.40 GeO_2 – 0.595 V_2O_5 – 0.005 Er_2O_3 glass with the heating rate of 10 °C/min.

As seen in DTA curves, there is only one exothermic peak is present for the thermally treated glass samples which are very close to the glass transition temperature therefore the crystallization stability of the glass is too low. After exothermic peak, one endothermic peak is demonstrated on the curve.

Characteristic temperatures and on-set crystallization temperatures (T_x) are given in Table 5.6. Glass transition temperature (T_g) lays at 209 ºC while crystallization peak temperatures (T_p) exist at 244 º and the melting temperatures (T_m) present at 631 °C.

Table 5.6 : Characteristic temperatures of the 0.595 GeO_2 - 0.40 V_2O_5 -0.005 Er_2O_3 glass

	0.40 GeO_2 – 0.595 V_2O_5 – 0.005 Er_2O_3			
T (°C)	T_g	T_x	T_{p1}	T_m
10 °C/min	209.5	238.06	244.13	631.33

5.8.2 XRD analysis of 0.40 GeO_2 – 0.595 V_2O_5 – 0.005 Er_2O_3 glass

In order to identify structural changes and phases in the microstructure of the 0.40 GeO_2 – 0.595 V_2O_5 – 0.005 Er_2O_3 , XRD investigations were performed.

Figure 5.24 shows the XRD pattern of as-cast and heat treated binary 0.40 GeO_2 – 0.595 V_2O_5 – 0.005 Er_2O_3 glass samples. The as-cast condition of pattern shows amorphous structure. The heat treated samples were prepared by water quenched right after the heating the as-cast glasses to 400°C for 2 hours with a 10°C/min heating rates. The annealing temperature was obtained from the DTA curves which is above the exothermic crystalline peak temperature

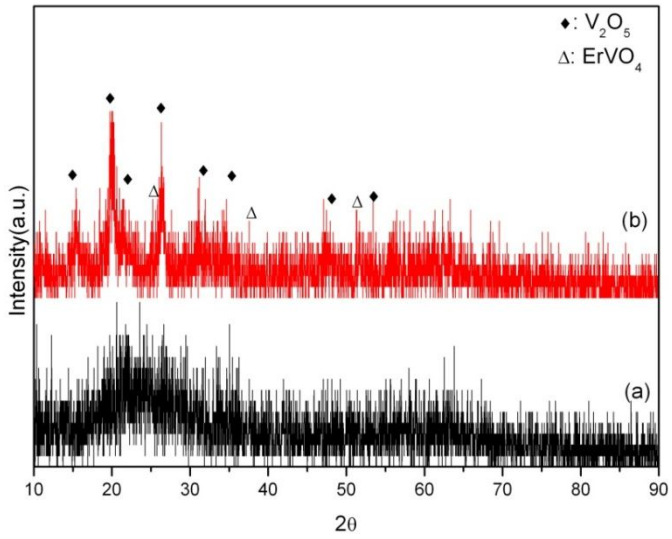

Figure 5.24 : XRD scans of the 0.40 GeO_2 – 0.595 V_2O_5– 0.005 Er_2O_3 glasses which are as-cast (a) and annealed at 400 °C

XRD pattern of annealed glass reveals the presence of the orthorhombic V_2O_5 and little amount of tetragonal $ErVO_4$ crystalline phases in its structure. The structures of the crystals, lattice parameters, space groups and card numbers of the crystalline phases observed in the glasses are given in Table B.1.

5.6.3 SEM investigations of the 0.40 GeO_2 – 0.595 V_2O_5 – 0.005 Er_2O_3 glass

SEM/SEI investigations were performed on the 0.40 GeO_2 – 0.595 V_2O_5 – 0.005 Er_2O_3 glasses in order to identify and analyze the morphology and size of the crystallizing phases. Figure 5.25(a) and (b) shows a series of SEM micrographs taken from the outer surface of the glass samples heated to 400 ◦C followed by quenching in water.

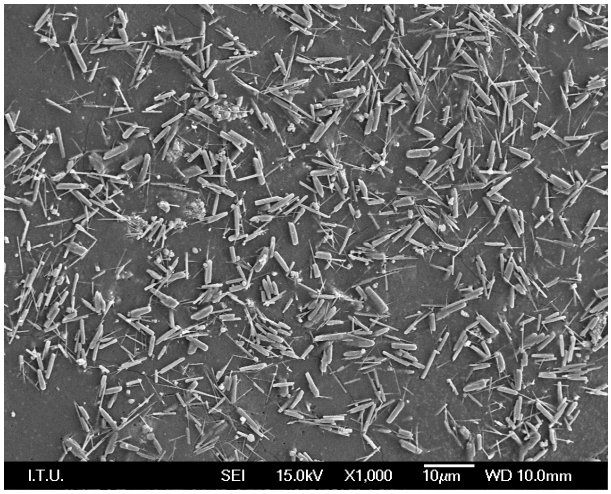

(a)

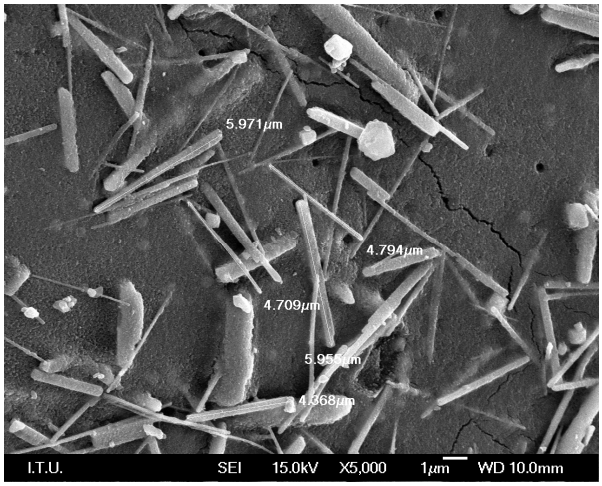

(b)

Figure 5.25 : SEM micrographs of the crystalline regions of the 0.40 GeO_2 – 0.595 V_2O_5 – 0.005 Er_2O_3 glass samples which was heat treated at 700 °C: (a) 1000x, (b) 5000x.

The micrographs demonstrate two different types of crystalline phases which are spread to glassy matrix. Even though Ge-based crystalline phase were not observed in the XRD pattern of the glass samples, formation of the germanium rich crystals which mainly reside at surface of the sample can be seen as needle -like crystals in

Figure 5.25 (a) and (b). EDS analyses were performed on the crystalline regions and revealed that (47.45 wt% Ge, 14.27 wt% V, 38.28 wt% O) needle-like crystals are Ge-rich crystals and can be belong to α-GeO_2 crystalline phase.

5.7 0.69 GeO_2 – 0.30 V_2O_5 – 0.01 Er_2O_3 Glass

As-cast 0.69 GeO_2 – 0.30 V_2O_5 – 0.01 Er_2O_3 glass samples are shown in Figure 5.26. As seen in Figure 5.26, as-cast 0.69 GeO_2 – 0.30 V_2O_5 – 0.01 Er_2O_3 glass samples have black color under visible light.

Figure 5.26 : As-cast 0.69 GeO_2 – 0.30 V_2O_5 – 0.01 Er_2O_3 glass samples

5.7.1 DTA investigations of the 0.69 GeO_2 – 0.30 V_2O_5 – 0.01 Er_2O_3 glass

DTA curve for the as cast 0.69 GeO_2 – 0.30 V_2O_5 – 0.01 Er_2O_3 glass with the heating rate of 10 °C/min is demonstrated in Figure 5.27.

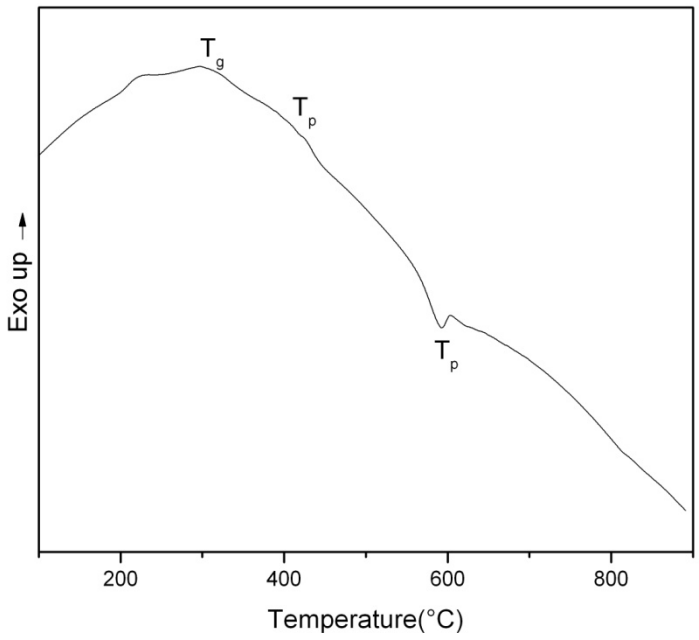

Figure 5.27 : DTA scan of the as-cast doped 0.69 GeO_2 – 0.30 V_2O_5 – 0.01 Er_2O_3 glass with the heating rate of 10 °C/min.

As seen in Figure 5.27, the DTA scans exhibit small endothermic peaks at 308°C as the glass transition temperature, T_g , and the melting temperatures (T_m) present at 591°C. Crystallization processes taking place in the glass matrix are marked by exothermic peak (T_p) at 424°C, indicating that the crystallization mechanism occurred for the glass samples. This thermal behavior were not observed for the other non-doped and 0.5 mol% Er_2O_3 doped glass samples which have the same composition of 0.69 GeO_2 – 0.30 V_2O_5 – 0.01 Er_2O_3 glass

Characteristic temperatures and on-set crystallization temperatures (T_x) are given in Table 5.7.

Table 5.7 : Characteristic temperatures of the 0.69 GeO_2 – 0.30 V_2O_5 – 0.01 Er_2O_3 glass

	0.69 GeO_2 – 0.30 V_2O_5 – 0.01 Er_2O_3			
T (°C)	T_g	T_x	T_{p1}	T_m
10 °C/min	308.09	417.36	424.13	591.56

5.7.2 XRD analysis of the 0.69 GeO_2 – 0.30 V_2O_5 – 0.01 Er_2O_3 glass

X-ray diffractometry scans were carried out on the basis of DTA results to identify the crystalline phases in the glasses which were annealed above the respective peak temperatures. XRD pattern of the 0.69 GeO_2 – 0.30 V_2O_5 – 0.01 Er_2O_3 glass samples were shown in Figure 5.28. The binary 0.69 GeO_2 – 0.30 V_2O_5 – 0.01 Er_2O_3 glass samples demonstrate some low intensity peaks which belong to $ErVO_4$ crystals in the as-cast condition as seem in Figure 5.28(a).

XRD pattern of the heat treated glass sample, which were annealed at 700°C for 2 hours with a heating rate of 10°C/min, indicated low intensity peaks of tetragonal β-GeO_2 crystalline phase in addition to the hexagonal GeO_2, orthorhombic V_2O_5 and tetragonal $ErVO_4$ crystalline phase.

The structures of the crystals, lattice parameters, space groups and card numbers of the crystalline phases, observed in the glasses are given in Table B 1.

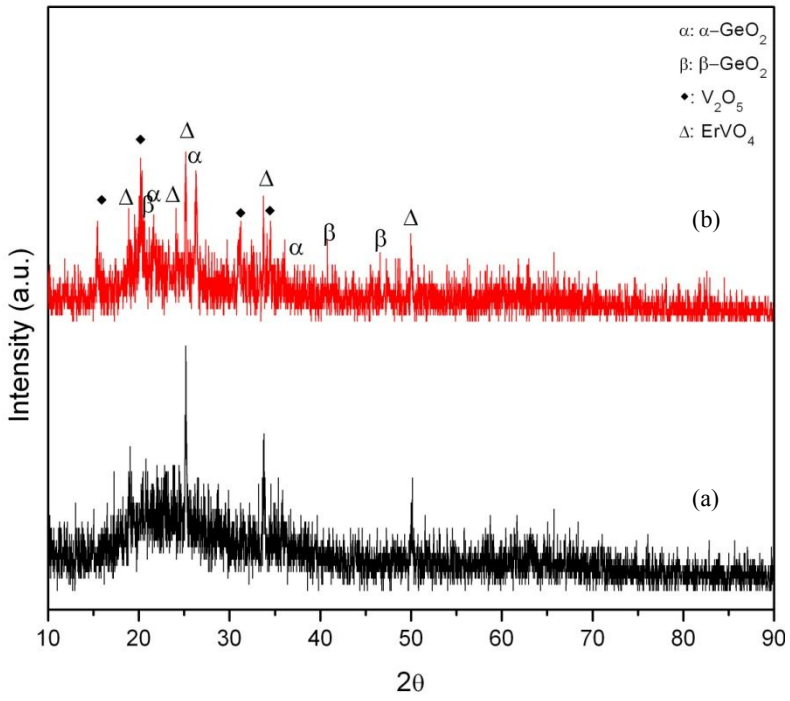

Figure 5.28 : XRD scans of the 0.69 GeO_2 – 0.30 V_2O_5 – 0.01 Er_2O_3 glasses which are as-cast (a) and annealed at 700 °C (b)

5.7.3 SEM investigations of the 0.69 GeO_2 – 0.30 V_2O_5 – 0.01 Er_2O_3 glass

SEM/SEI investigations were performed on the 0.69 GeO_2 – 0.30 V_2O_5 – 0.01 Er_2O_3 glasses in order to identify and analyze the morphology and size of the crystallizing phases. Figure 5.29 (a) and (b) shows a series of the SEM micrographs taken from the outer surface of the glass samples heated to 500 ◦C for 2 hours with a heating rate of 10°C/min followed by quenching in water.

Formation of the vanadium rich crystals which mainly reside at cross section of the sample can be seen as icicle-like structure in Figure 5.29 (b). In addition to these structures, formation of vanadium and erbium rich crystals is also observed as sphere like crystals which is 0.2-0.35 μm in size, in Figure 5.29 (a).

EDS analyses were performed on the crystalline regions (Figure 5.29(b)) and revealed that (10.03 wt% Ge, 43.44 wt% V, 65.56 wt% O) icicle-like structures belong to V_2O_5 crystalline phase. The sphere- like crystalline regions (Figure 5.29 (a)) indicate that (1.88 wt% Ge, 22.06 wt% V, 55.63 wt% O, 20.12 wt% Er) these structures consist of $ErVO_4$ crystals.

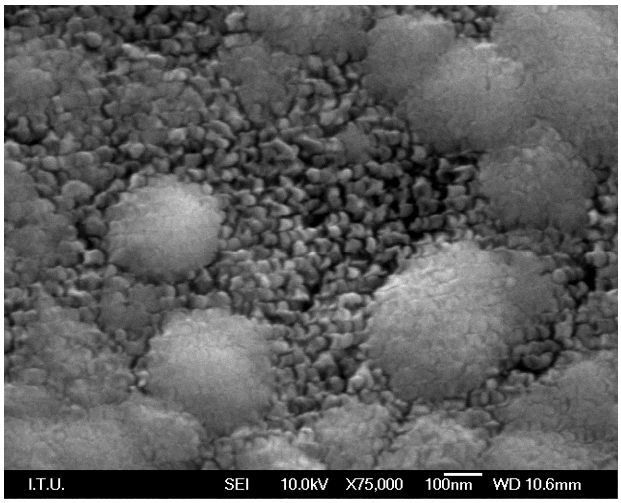

(a)

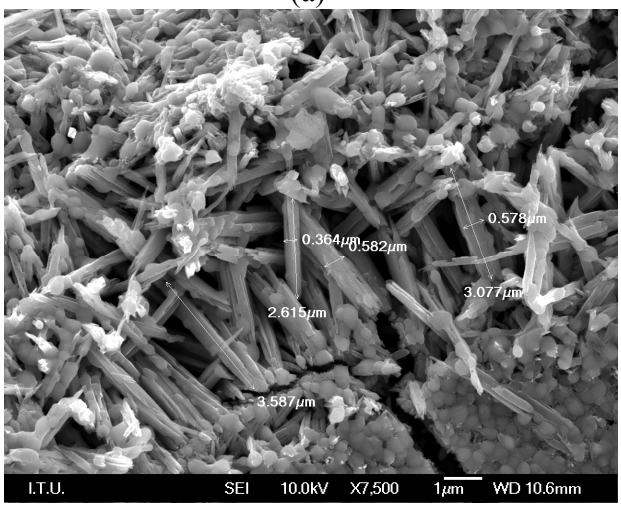

(b)

Figure 5.29 : SEM micrographs of the crystalline regions of the 0.69 GeO_2 – 0.30 V_2O_5 – 0.01 Er_2O_3 glass samples which was heat treated at 700 °C: (a) 75000x, (b) 7500x.

5.8 0.57 GeO_2 – 0.42 V_2O_5 – 0.01 Er_2O_3 Glass

As-cast 0.57 GeO_2 – 0.42 V_2O_5 – 0.01 Er_2O_3 glass samples are shown in Figure 5.30. As seen in Figure 5.30, as-cast 0.57 GeO_2 – 0.42 V_2O_5 – 0.01 Er_2O_3 glass samples have black color under visible light.

Figure 5.30 : As-cast 0.57 GeO_2 – 0.42 V_2O_5 – 0.01 Er_2O_3 glass samples

5.8.1 DTA investigations of the 0.57 GeO_2 – 0.42 V_2O_5 – 0.01 Er_2O_3 glass

Differential thermal (DTA) investigations were conducted on the as-cast 0.575 GeO_2 – 0.42 V_2O_5 – 0.005 Er_2O_3 glasses. Figure 5.31 shows the respective DTA data of the as-cast glass samples scanned at a rate of 10°C/min between 100 and 900°C.

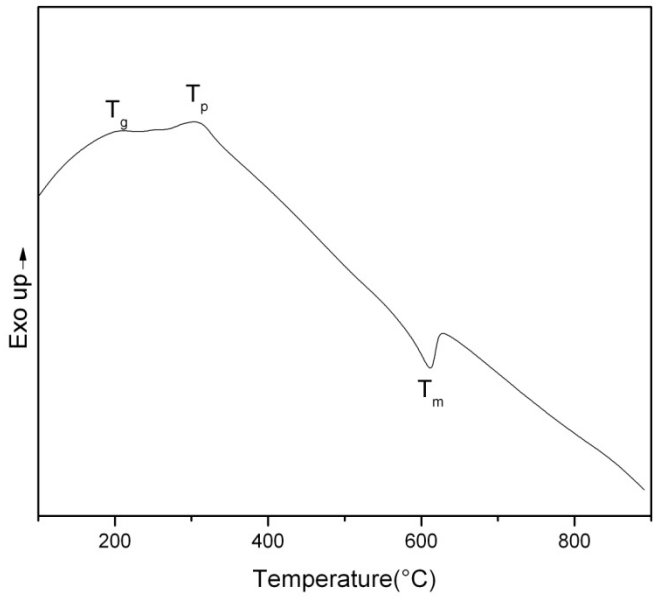

Figure 5.31 : DTA scan of the as-cast doped 0.57 GeO_2 – 0.42 V_2O_5 – 0.01 Er_2O_3 glass with the heating rate of 10 °C/min.

As seen in Figure 5.31, the DTA scans exhibit small endothermic peaks at 212°C as the glass transition temperature, (T_g) , and wide endothermic peak at 612 °C as the melting temperatures (T_m). Crystallization processes taking place in the glass matrix are marked by exothermic peak (T_p) at 303°C, indicating that the crystallization mechanism occurred for the glass samples.

Characteristic temperatures and on-set crystallization temperatures (T_x) are given in Table 5.8.

Table 5.8 : Characteristic temperatures of the 0.57 GeO_2 – 0.42 V_2O_5 – 0.01 Er_2O_3 glass.

	0.57 GeO_2 – 0.42 V_2O_5 – 0.01 Er_2O_3			
T (°C)	T_g	T_x	T_{p1}	T_m
10 °C/min	212.64	277.97	303.21	612.69

5.8.2 XRD analysis of 0.57 GeO_2 – 0.42 V_2O_5 – 0.01 Er_2O_3 glass

On the basis of DTA results, X-ray diffractometry scans were applied to verify the nature of crystallizing phase in the glassy matrix. Fifure 5.32 shows the XRD pattern of the 0.575 GeO_2 – 0.42 V_2O_5 – 0.005 Er_2O_3 glasses in the as-cast condition and crystallized glass.

X-ray diffractometry patterns of the as-cast 0.575 GeO_2 – 0.42 V_2O_5 – 0.005 Er_2O_3 glasses revealed no detectable peaks, confirming that they consist of only amorphous glass matrix (Figure 5.32(a)).

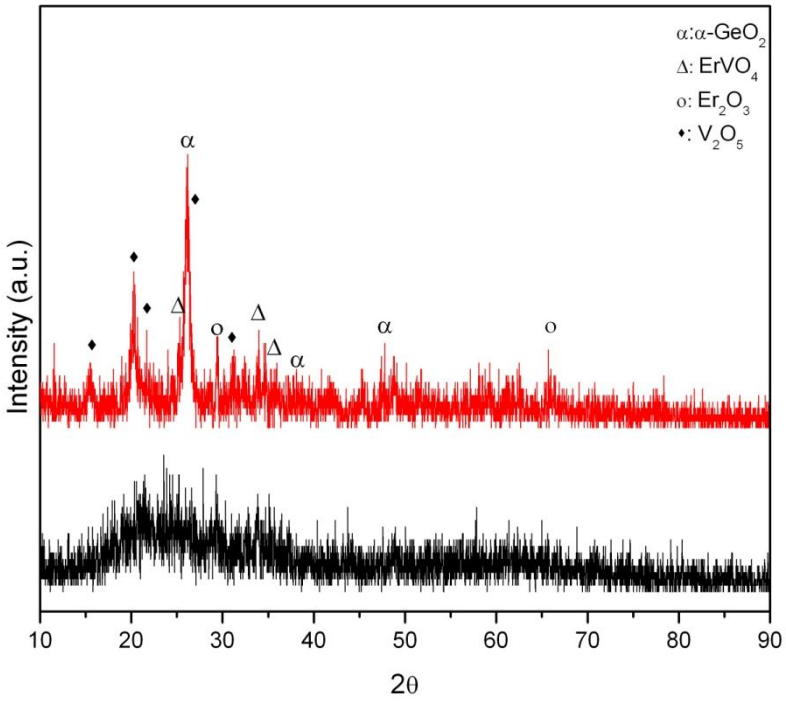

Figure 5.32 : XRD scans of the 0.69 GeO_2 – 0.30 V_2O_5 – 0.01 Er_2O_3 glasses which are as-cast (a) and annealed at 700 °C (b)

XRD pattern of the heat treated glass sample, which were annealed at 400°C for 2 hours with a heating rate of 10°C/min, indicated low intensity peaks of cubic Er_2O_3 crystalline phase in addition to the tetragonal $ErVO_4$, the hexagonal GeO_2 and orthorhombic V_2O_5 crystalline phases. The structures of the crystals, lattice parameters, space groups and card numbers of the crystalline phases, observed in the glasses are given in Table B 1.

5.8.3 SEM investigations of the 0.57 GeO_2 – 0.42 V_2O_5 – 0.01 Er_2O_3 glass

SEM/SEI investigations were performed on the 0.57 GeO_2 – 0.42 V_2O_5 – 0.01 Er_2O_3 glasses in order to identify and analyze the morphology and size of the crystallizing phases. Figure 5.33(a) and (b) shows a series of the SEM micrographs taken from the outer surface of the glass samples heated to 400 ◦C for 2 hours with a heating rate of 10°C/min followed by quenching in water.

The micrographs demonstrate four different types of crystalline phases which are thin and thick needle-like, blocky-shaped, little spheroid shaped crystals.

Formation of the vanadium rich crystals which are 20-40 nm in size can be seen in Figure 5.33 (b) and (c). EDS analyses were performed on the crystalline regions and revealed that (0.57 GeO_2 – 0.42 V_2O_5 – 0.01 Er_2O_3) little spheroid shaped crystals are V-rich crystals and according to XRD results these crystals can be identified as V_2O_5 crystalline phase.

As seen from the Figure5.33 (c) and (d) thin and thick needle like crystals which were observed in SEM micrographs of the 0.57 GeO_2 – 0.42 V_2O_5 – 0.01 Er_2O_3 glasses too, are very small quantities and scattered in the parent glassy matrix. EDS spectra taken from the thin and thick needle like crystalline structures and show that thin needle-like structures contained 21.06 wt% Ge, 15.93 wt% V, 62.36 wt% O and 0.65 wt% Er and thick needle like structures contained 36.82 wt% Ge, 6.33 wt% V, 56.75 wt% O, 0.65 wt% Er , indicating the fact that they are germanium rich crystals.

In addition to these structures, Figure 5.33(a) demonstrates blocky shaped structures which were 0.2-0.9 μm in size. EDS analyses were performed on the crystalline regions and revealed that (10.03 wt% Ge, 43.44 wt% V, 65.56 wt% O) block-shaped structures belong to $ErVO_4$ crystalline phase, also were detected in XRD scans.

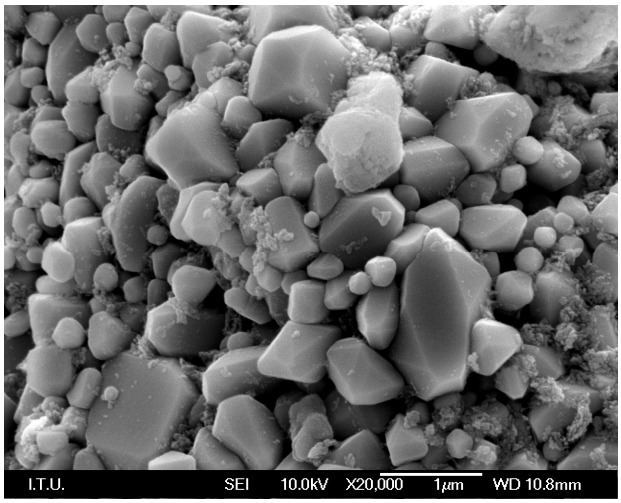

(a)

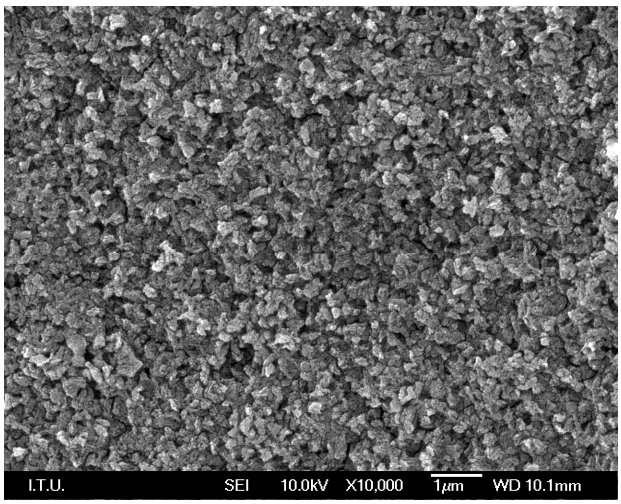

(b)

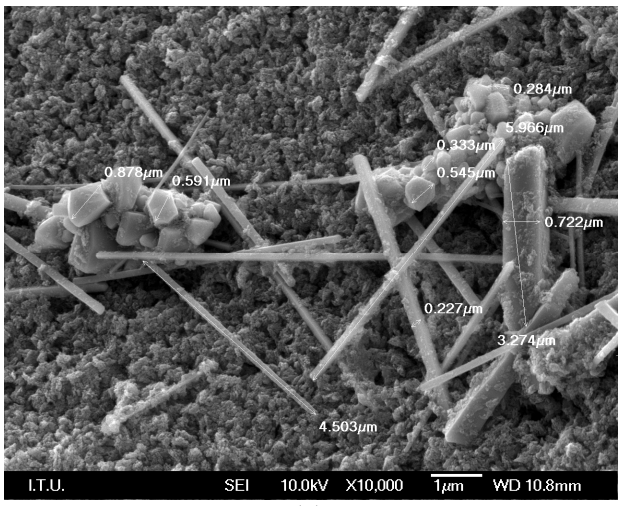

(c)

Figure 5.33 : SEM micrographs of the crystalline regions of the 0.57 GeO_2 – 0.42 V_2O_5 – 0.01 Er_2O_3 glass samples which was heat treated at 700 °C: (a) 20000x, (b) 10000x, (c) 10000x.

5.9 0.40 GeO_2 – 0.59 V_2O_5 – 0.01 Er_2O_3 Glass

As-cast 0.40 GeO_2 – 0.59 V_2O_5 – 0.01 Er_2O_3 glass samples are shown in Figure 5.34. As seen in Figure 5.34, as-cast 0.40 GeO_2 – 0.59 V_2O_5 – 0.01 Er_2O_3 glass samples have black color under visible light.

Figure 5.34 : As-cast 0.40 GeO_2 – 0.59 V_2O_5 – 0.01 Er_2O_3 glass samples

5.9.1 DTA investigations of the 0.40 GeO_2 – 0.59 V_2O_5 – 0.01 Er_2O_3 glass

Differential thermal (DTA) investigations were conducted on the as-cast 0.40 GeO_2 – 0.59 V_2O_5 – 0.01 Er_2O_3 glasses. Figure 5.35 shows the respective DTA data of the as-cast glass samples scanned at a rate of 10°C/min between 100 and 900°C.

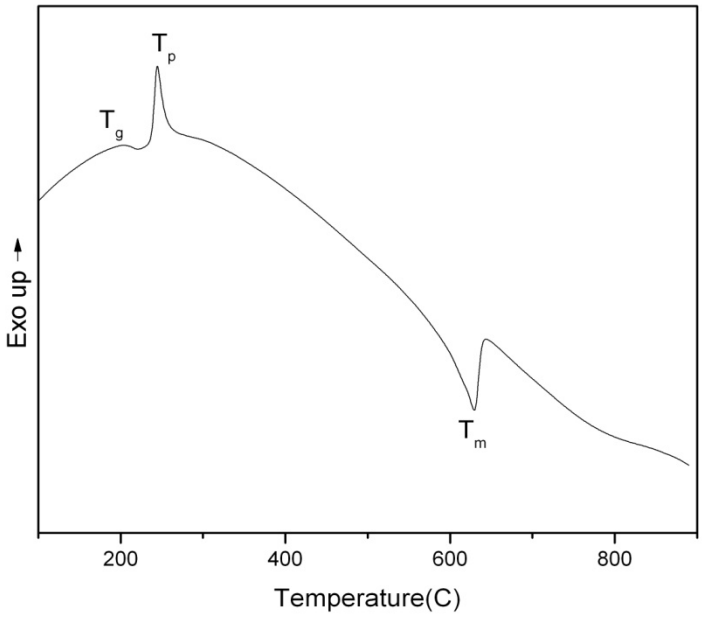

Figure 5.35 : DTA scan of the as-cast doped 0.40 GeO_2 – 0.59 V_2O_5 – 0.01 Er_2O_3 glass with the heating rate of 10 °C/min.

As seen in Figure 5.35, the DTA scans exhibit small endothermic peaks at 208°C as the glass transition temperature, T_g , and wide endothermic peak at 629 °C as the melting temperatures (T_m). Crystallization processes taking place in the glass matrix

are marked by exothermic peak (T_p) at 244°C, indicating that the crystallization mechanism occurred for the glass samples. Characteristic temperatures and on-set crystallization temperatures (T_x) are given in Table 5.9.

Table 5.9: Characteristic temperatures of the 0.40 GeO_2 – 0.59 V_2O_5 – 0.01 Er_2O_3 glass.

0.40 GeO_2 – 0.59 V_2O_5 – 0.01 Er_2O_3				
T (°C)	T_g	T_x	T_{p1}	T_m
10 °C/min	208.85	235.97	244.5	629.69

5.9.2 XRD analysis of 0.40 GeO_2 – 0.59 V_2O_5 – 0.01 Er_2O_3 glass

X-ray diffractometry scans were carried out on the basis of DTA results to identify the crystalline phases in the glasses which were annealed above the respective peak temperatures. The binary 0.40 GeO_2 – 0.59 V_2O_5 – 0.01 Er_2O_3 glass samples demonstrate some low intensity peaks which belong to $ErVO_4$ crystals in the as-cast condition as seem in Figure 5.36(a).

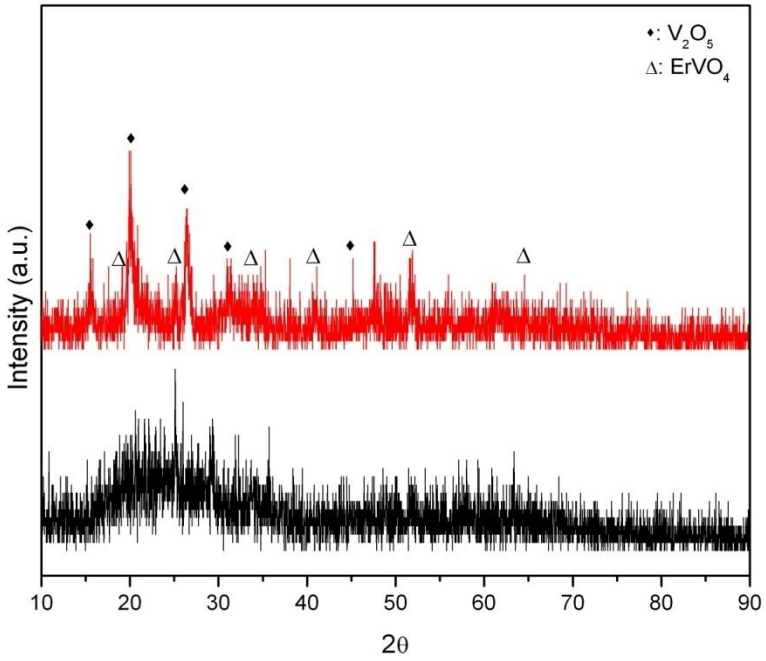

Figure 5.36 : XRD scans of the 0.40 GeO_2 – 0.59 V_2O_5 – 0.01 Er_2O_3 glasses which are as-cast (a) and annealed at 400 °C (b)

XRD pattern of the heat treated glass sample, which were annealed at 400°C for 2 hours with a heating rate of 10°C/min, indicated the orthorhombic V_2O_5 and the tetragonal $ErVO_4$ crystalline phase.

The structures of the crystals, lattice parameters, space groups and card numbers of the crystalline phases, observed in the glasses are given in Table B 1.

5.9.3 SEM investigations of the 0.40 GeO_2 – 0.59 V_2O_5 – 0.01 Er_2O_3 glass

SEM/SEI investigations were performed on the 0.40 GeO_2 – 0.59 V_2O_5 – 0.01 Er_2O_3 glasses in order to identify and analyze the morphology and size of the crystallizing phases. Figure 5.37 (a)–(b) shows a series of the SEM micrographs taken from the outer surface of the glass samples heated to 400 ◦C for 2 hours with a heating rate of 10°C/min followed by quenching in water.

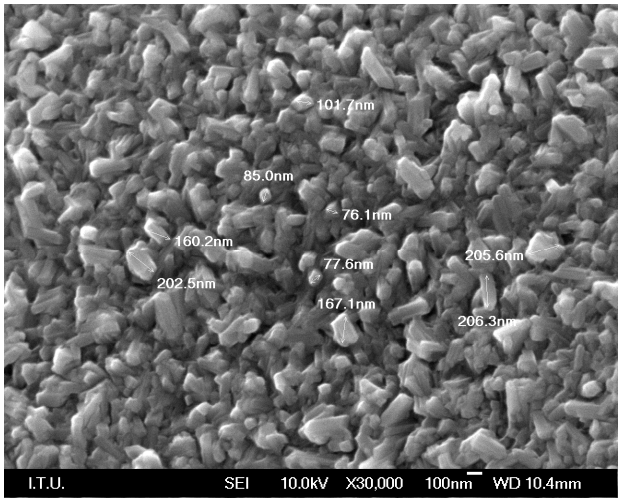

(a)

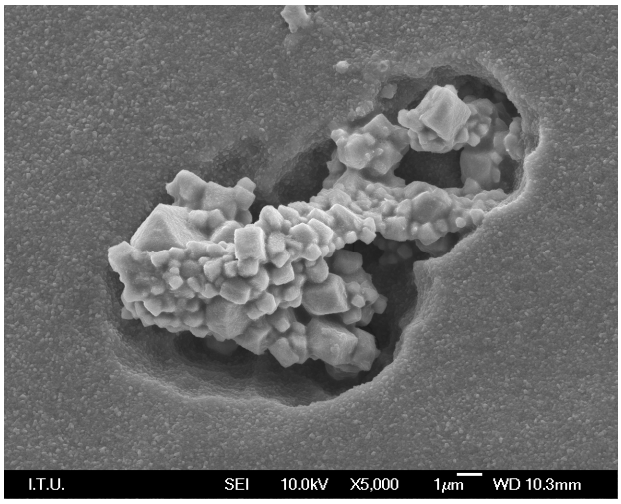

(b)

Figure 5.37 : SEM micrographs of the crystalline regions of the 0.40 GeO_2 – 0.59 V_2O_5 – 0.01 Er_2O_3 glass samples which was heat treated at 700 °C : (a) 30000x, (b) 5000x.

Figure 5.37 (b) are representative SEM micrographs which reveal the presence of blocky-shaped crystals varying between 0.3- 0.8 μm in size. EDS spectra taken from these blocky-shaped crystalline regions revealed that they contained 3.07 wt% Ge, 18.58 wt% V, 52.56 wt% O and 25.78 wt% Er , which suggesting that they are $ErVO_4$ crystals also detected in XRD scans. Same morphology were observed in the SEM micrographs of the 0.57 GeO_2 – 0.42 V_2O_5 – 0.01 Er_2O_3 glass samples and the results of the EDS spectra are correspond to the each other.

In addition to blocky-shaped structures, the oblongished shaped structures which are spread to the surface of the glass samples, can be observed from the Figure 5.37 (a). EDS analyses taken from these crystalline region revealed that they contained 11.71 wt% Ge, 22.53 wt% V, 65.76 wt% O, suggesting that they are vanadium rich regions. Based on the XRD results of the glass samples we can named these crystals as V_2O_5 crystals

5.10 Discussion

DTA investigations were conducted on the as-cast binary doped and non-doped glass system to understand the effect of V_2O_5 content on the thermal behavior of the glasses. The respective DTA thermogram with 10°C/min heating rate was given in Figure 5.38-5.40.

Based on DTA scans which were shown in Figure 5.38, the addition of V_2O_5 content into the glass structure lowers the glass transition temperature. These results suggest that V_2O_5 acts as a network modifier and GeO_2 acts as a network former in the network structure (Tatar and Öveçoğlu, 2009; Tatar et al., 2009). The melting peak temperatures changed irreularly with increasing V_2O_5 content. Eutectic composition has the lowest value of the melting peak temperature while the hypereutectic and hypoeutectic compositions of the binary glass systems have the almost same value. Table 5.10 shows all characteristic temperatures for non-doped and doped GeO_2-V_2O_5 binary glass system with heating rate of 10°C/min.

DTA curves of binary glass system with 30mol% V_2O_5 content show no clear exothermic peaks on their DTA curves which suggest that these system have excellent thermal stability against crystallization. Further V_2O_5 content evoke crystallization peak for the 0.58 GeO_2 – 0.42 V_2O_5 and 0.40 GeO_2 – 0.60 V_2O_5 glass samples. Addition of V_2O_5 content decreases the exothermic peak temperatures while increases the peak areas with small amount as shown in the Figure 5.38.

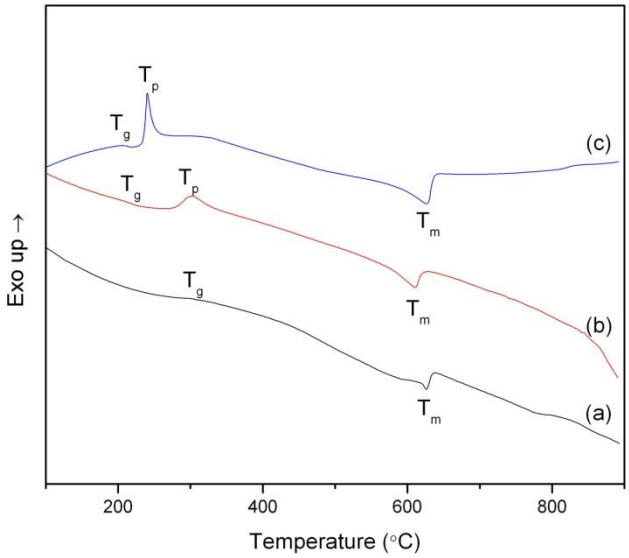

Figure 5.38 : DTA scans of the as-cast non-doped 0.70 GeO_2 – 0.30 V_2O_5 (a), 0.58 GeO_2 – 0.42 V_2O_5 (b), 0.40 GeO_2 – 0.60 V_2O_5 (c) glasses with a heating rate of 10 °C/min

Thermal effects of different V_2O_5 contents on GeO_2 – V_2O_5 glass system doped with 0. 5 mol% Er_2O_3 can be seen in Figure 5.39.

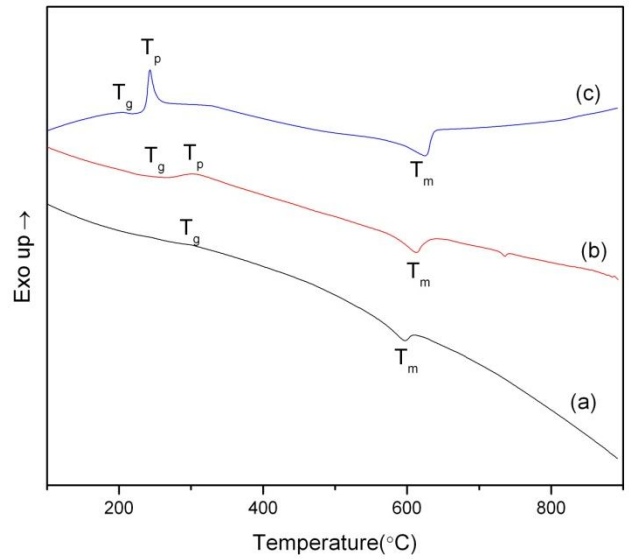

Figure 5.39 :DTA scans of the as-cast doped 0.695 GeO_2 – 0.30 V_2O_5 – 0.005 Er_2O_3 (a), 0.575 GeO_2 – 0.42 V_2O_5 – 0.005 Er_2O_3 (b), 0.40 GeO_2 – 0.595 V_2O_5 – 0.005 Er_2O_3 (c) glasses with a heating rate of 10 °C/min

There is no detectable exothermic peak were observed from the DTA curves of the 0.695 GeO_2 – 0.30 V_2O_5 – 0.005 Er_2O_3 glass samples while the 0.575 GeO_2 – 0.42 V_2O_5 – 0.005 Er_2O_3 and the 0.40 GeO_2 – 0.595 V_2O_5 – 0.005 Er_2O_3 glass samples have one exothermic peak on their curves. As a result, it is right to say that glass samples show tendency for crystallizing with increment of V_2O_5 content. In addition

to that, the exothermic peak shift to lower values and the exothermic peak becomes sharper with increasing V_2O_5 content. It is also noticed that the glass transition temperatures tend to decrease with increasing V_2O_5 content and while the melting peak temperatures increase with increasing V_2O_5 content.

Thermal effects of different V_2O_5 contents on $GeO_2 – V_2O_5$ glass system doped with 1 mol% Er_2O_3 can be seen in Figure 5.40. There is no detectable exothermic peak were observed from the DTA curves of the 0.69 GeO_2 – 0.30 V_2O_5 – 0.01 Er_2O_3 glass samples while the 0.57 GeO_2 – 0.42 V_2O_5 – 0.01 Er_2O_3 and the 0.40 GeO_2 – 0.59 V_2O_5 – 0.01 Er_2O_3 glass samples have one exothermic peak on their curves. As a result, it is right to say that glass samples show tendency for crystallizing with increment of V_2O_5 content. In addition to that, the exothermic peak shift to lower values and the exothermic peak becomes sharper with increasing V_2O_5 content. It is also noticed that the glass transition temperatures and the melting peak temperatures tend to decrease with increasing V_2O_5 content while the melting peak temperatures increase with the increment of V_2O_5 content.

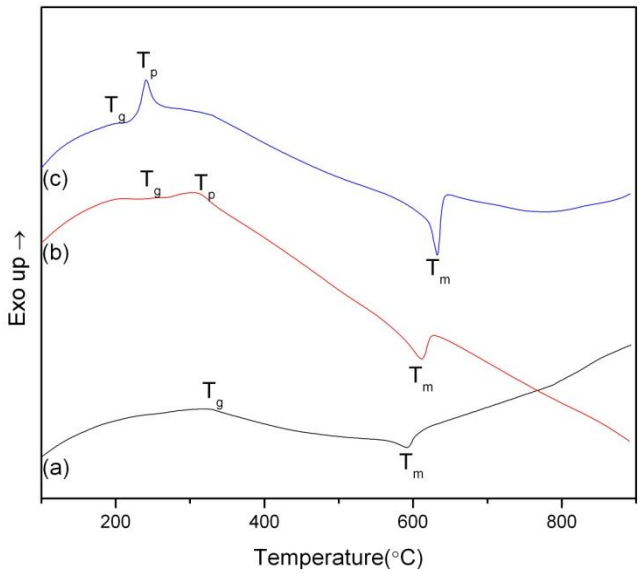

Figure 5.40 : DTA scans of the 0.69 GeO_2 – 0.30 V_2O_5 – 0.01 Er_2O_3 (a), 0.57 GeO_2 – 0.42 V_2O_5 – 0.01 Er_2O_3 (b), 0.40 GeO_2 – 0.59 V_2O_5 – 0.01 Er_2O_3 (c) glasses with a heating rate of 10 °C/min

Figure 5.41 shows to the DTA curves for the as-cast (0.70 – y) GeO_2 – 0.30 V_2O_5 – y Er_2O_3 (y = 0, 0.005, 0.01) glasses with the heating rate of 10 °C/min. As seen from the Figure 5.41, the glass transition temperatures and melting temperatures decrease to lower temperatures with the addition of erbium content for both doped and non-doped glass samples. As seen from the Figure 5.41 for both non-doped and doped

with 0.005 mol% Er_2O_3 content glass samples has no clear exothermic peak while the existence of slight exothermic peak can be observed for the 0.69 GeO_2 – 0.30 V_2O_5 – 0.01 Er_2O_3 glass samples. This situation can be associated with new crystalline phase formation with introduction of erbium content.

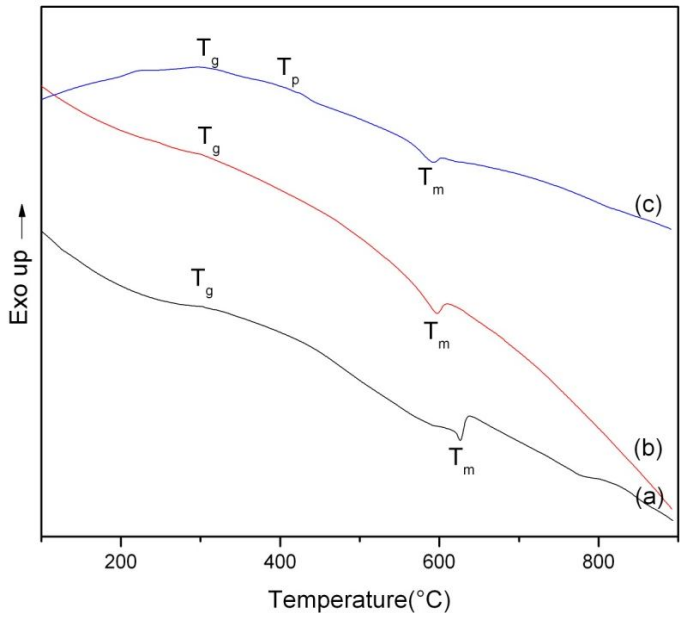

Figure 5.41 : DTA scans of the 0.70 GeO_2 – 0.30 V_2O_5 (a), 0.695 GeO_2 – 0.30 V_2O_5 – 0.005 Er_2O_3(b), 0.69 GeO_2 – 0.30 V_2O_5 – 0.01 Er_2O_3(c) glasses with a heating rate of 10 °C/min.

Figure 5.42 represents the respective DTA curves of the as-cast (0.58 – y) GeO_2 – 0.42 V_2O_5 – y Er_2O_3 (y = 0. 0.005) glasses scans at rate of 10 °C/min. As seen in Figure 5.42, each DTA scan exhibits exothermic crystallization peak, endothermic melting peak and small endothermic peak corresponding to the glass transition temperature which remain the same value for doped and non-doped binary glass system with addition of erbium content.

Even the peak temperatures have the almost same value, the exothermic and endothermic peak areas shows little bit difference for the doped and non-doped binary glass system.

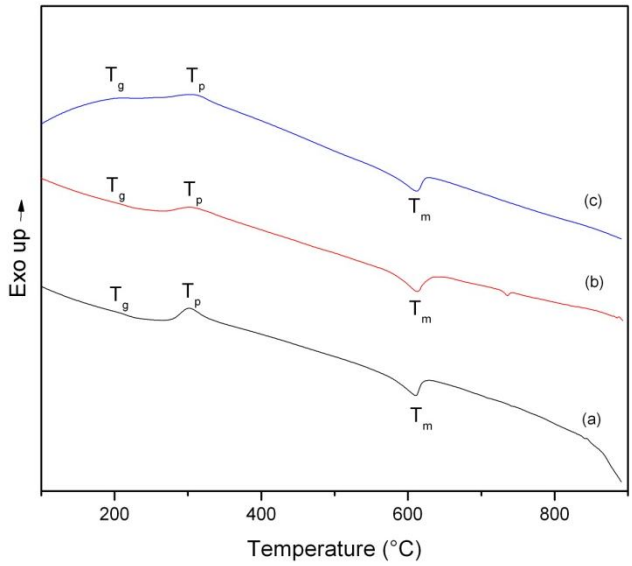

Figure 5.42 : DTA scans of the 0.58 GeO_2 – 0.42 V_2O_5 (a), 0.575 GeO_2 – 0.42 V_2O_5 – 0.005 Er_2O_3(b), 0.57 GeO_2 – 0.42 V_2O_5 – 0.01 Er_2O_3(c) glasses with a heating rate of 10 °C/min

On the basis of DTA results, it can be inferred that the addition of Er_2O_3 content has no big effect on the thermal properties of the 0.40 GeO_2 – 0.60 V_2O_5 doped and non-doped binary glasses. As seen from Figure 5.43, the glass transition temperature, endothermic melting peak temperature and the exothermic peak temperature have the almost same value for the binary doped and non-doped glass systems. Only effect of the increasing erbium content can be seen in the exothermic peak areas which are induced to become larger with introduction of the erbium content.

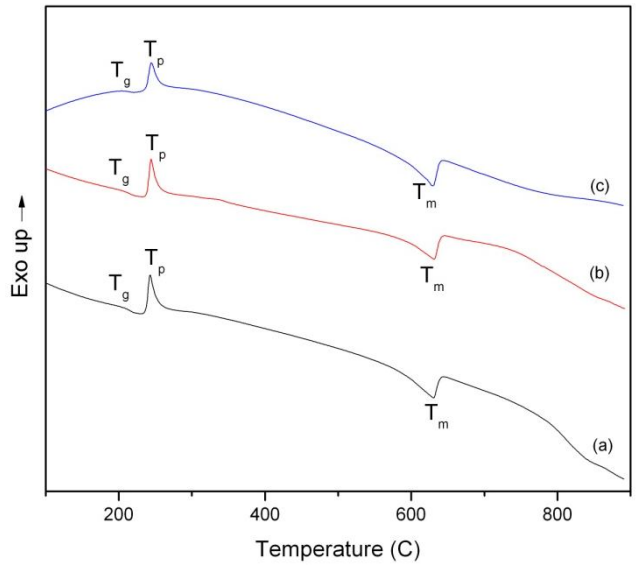

Figure 5.43 : DTA scans of the 0.40 GeO_2 – 0.60 V_2O_5 (a), 0.40 GeO_2 – 0.595 V_2O_5 – 0.005 Er_2O_3(b), 0.40 GeO_2 – 0.59 V_2O_5 – 0.01 Er_2O_3(c) glasses with a heating rate of 10 °C/min

Table 5.10 demonstrates the characteristic temperatures for doped and non-doped binary vanadium germanate glass system. The general results of thermal properties for the glass transition temperature and crystallization temperature show decrease with increasing V_2O_5 content. Decreasing of glass transition temperature makes decreasing at rigidity on network and means that more open network is seen (A. Abd El Moneim, 2001).

The temperature difference between the T_g and the first exothermic peak T_{p1}, $\Delta T = T_{p1} - T_g$, gives a measure for the thermal stability of the glass against crystallization. ΔT represents the temperature interval during which nucleation takes place (Murugan and Ohishi, 2004). The calculated value of thermal stability for 0.58 GeO_2-0.42 V_2O_5 glass sample is 86.91°C and 0.40 GeO_2-0.60 V_2O_5 glass sample has lowest value of 32°C while the calculation of 30 mol% V_2O_5 content glass are impossible because the DTA curves do not demonstrate any exothermic crystallization peak.

Table 5.10 : Characteristic temperatures of the non-doped and doped GeO_2 – PbF_2 glasses for heating rate of 10 °C/min

Compositions (mol)	**T_g (°C)**	**T_x(°C)**	**T_p(°C)**	**T_m(°C)**
0.70 GeO_2 – 0.30 V_2O_5	308.40	*	*	626.44
0.695 GeO_2 – 0.3 V_2O_5 – 0.005 Er_2O_3	304.05	*	*	595.88
0.69 GeO_2 – 0.3 V_2O_5 – 0.01 Er_2O_3	302.09	417.36	424.13	591.56
0.58 GeO_2 – 0.42 V_2O_5	218.13	278.34	301.49	610.29
0.575 GeO_2 – 0.42 V_2O_5 – 0.005 Er_2O_3	217.10	275.97	301.21	612.35
0.57 GeO_2 – 0.42 V_2O_5 – 0.01 Er_2O_3	212.64	277.97	303.21	612.69
0.40 GeO_2 – 0.60 V_2O_5	209.14	236.87	242.67	630.30
0.40 GeO_2 – 0.595 V_2O_5 – 0.005 Er_2O_3	208.65	238.06	244.13	631.33
0.40 GeO_2 – 0.59 V_2O_5 – 0.01 Er_2O_3	208.56	235.97	244.51	629.69

Figure 5.44 demonstrate the XRD pattern of the binary GeO_2-V_2O_5 annealed glass samples which include 30 mol%, 42mol% and 60mol% V_2O_5 content. XRD pattern of annealed non-doped 0.7 GeO_2 – 0.3 V_2O_5 glass sample indicated the presence of hexagonal GeO_2 phase and orthorhombic V_2O_5 crystalline phase. As V_2O_5 content increases from 30mol% to 42mol%, causes to crystallized α-GeO_2 to sudden decrease while the amount of V_2O_5 phase increase.

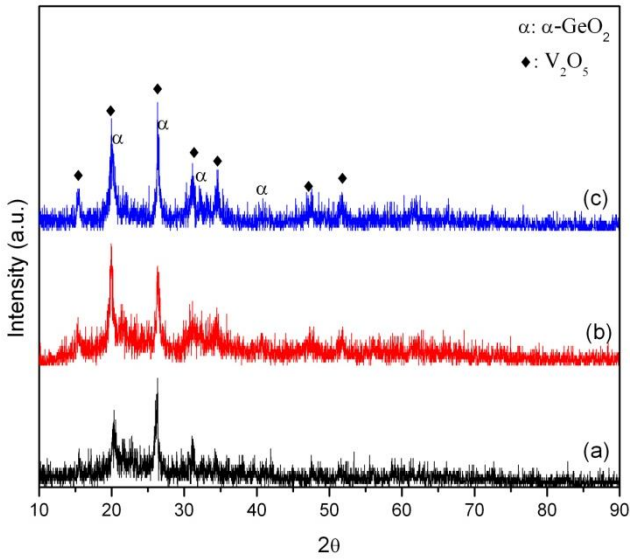

Figure 5.44 : XRD scans of the 0.7 GeO_2 – 0.30 V_2O_5 (a), 0.58 GeO_2 – 0.42 V_2O_5 (b), 0.40 GeO_2 – 0.60 V_2O_5 (c) non-doped glasses which are annealed at 500°C ,400°C and 400°C, respectively.

Figure 5.45 demonstrate the XRD pattern of the binary GeO_2-V_2O_5 annealed glass samples which include 10mol%, 30 mol%, 42mol% and 60mol% V_2O_5 content and doped with 0.5 mol% Er_2O_3. XRD pattern of annealed doped 0.7 GeO_2 – 0.3 V_2O_5 glass sample indicated the presence of hexagonal GeO_2, tetragonal GeO_2 and the orthorhombic V_2O_5 crystalline phase in addition to high amount of tetragonal $ErVO_4$ crystalline phase.

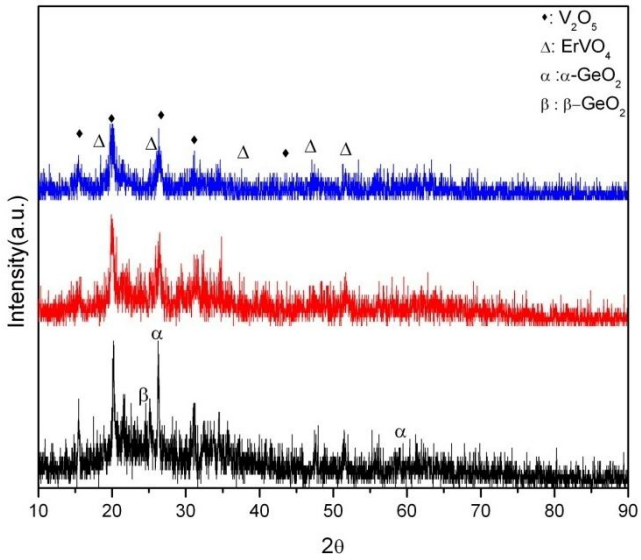

Figure 5.45 :XRD scans of the 0.695 GeO_2 – 0.30 V_2O_5 – 0.005 Er_2O_3 (a), 0.575 GeO_2 – 0.42 V_2O_5 – 0.005 Er_2O_3 (b), 0.40 GeO_2 – 0.595 V_2O_5 – 0.005 Er_2O_3 (c) doped glasses which are annealed at 500°C ,400°C and 400°C, respectively.

As V_2O_5 content increases from 30mol% to 42mol%, the crystallized β-GeO_2 phase disappears from the XRD pattern while the intensity of the V_2O_5 crystalline phase increased. For all composition of doped binary glass system $ErVO_4$ phase is observed. Further increment of the V_2O_5 content causes to crystallized α-GeO_2 to sudden decrease while the amount of V_2O_5 phase and $ErVO_4$ phase increase.

Figure 5.46 demonstrate the XRD pattern of the binary GeO_2-V_2O_5 annealed glass samples which include 30 mol%, 42mol% and 60mol% V_2O_5 content and doped with 1 mol% Er_2O_3.

XRD pattern of annealed doped 0.7 GeO_2 – 0.3 V_2O_5 glass sample indicated the presence of hexagonal GeO_2, tetragonal GeO_2 and the orthorhombic V_2O_5 crystalline phase in addition to high amount of tetragonal $ErVO_4$ crystalline phase.

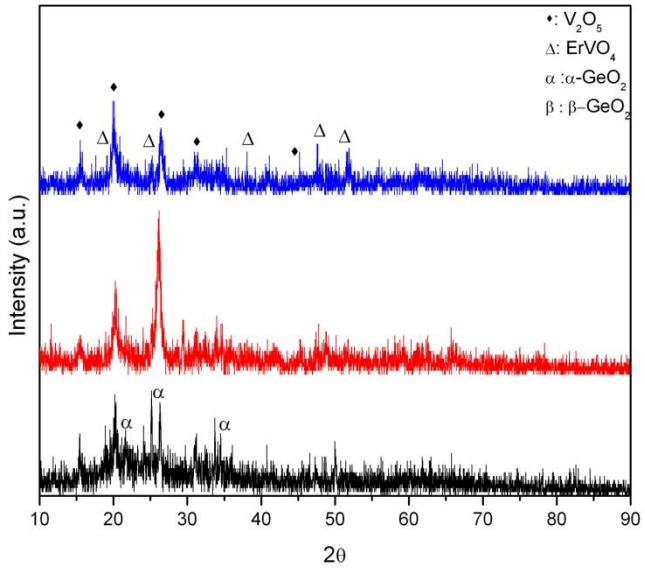

Figure 5.46 :XRD scans of the 0.69 GeO_2 – 0.30 V_2O_5 – 0.01 Er_2O_3 (a), 0.57 GeO_2 – 0.42 V_2O_5 – 0.01 Er_2O_3 (b), 0.40 GeO_2 – 0.59 V_2O_5 – 0.01 Er_2O_3 (c) doped glasses which are annealed at 500°C ,400°C and 400°C, respectively.

As V_2O_5 content increases from 30mol% to 42mol%, the crystallized β-GeO_2 phase disappears from the XRD pattern while the intensity of the V_2O_5 crystalline phase increased. For all composition of doped binary glass system $ErVO_4$ phase is observed. Further increment of the V_2O_5 content causes to crystallized α-GeO_2 to sudden decrease while the amount of V_2O_5 phase and $ErVO_4$ phase increase.

6. CONCLUSION AND RECOMMENDATIONS

1. All glass samples show amorphous clustering and they have black color under visible light.

2. The glass transition temperatures decrease with increasing V_2O_5 content 30 mol% to 60 mol%. This indicates that V_2O_5 acts as a network modifier and GeO_2 acts as a network former in the structure.

3. For both non-doped and 0.5 mol% Er_2O_3 doped glass samples with 30 mol% V_2O_5 content has no clear exothermic peak while the existence of slight exothermic peak are observed for the 0.69 GeO_2 – 0.30 V_2O_5 – 0.01 Er_2O_3 glass samples. This situation can be associated with new crystalline phase formation with introduction of erbium content. In addition to that glass samples with 42 mol% and 60 mol% V_2O_5 content have intense exothermic peaks right after glass transition temperature. This affirms thermal stability of these glasses decreases with increasing V_2O_5 content.

4. The glass transition temperature affected slightly by erbium content in studied GeO_2 – V_2O_5 glasses.

5. Erbium doped and non-doped binary GeO_2 – V_2O_5 glass system accommodates four different crystalline phase which are α-GeO_2, β-GeO_2, V_2O_5, and $ErVO_4$. As V_2O_5 content increased to 42 mol%, a sudden decrease on nucleation of β-GeO_2 phase is observed in doped GeO_2 – V_2O_5 glasses. With more increment of V_2O_5 content, intensities of α-GeO_2 phase decreases while intensity of V_2O_5 phase increases.

6. SEM/SEI micrographs of non-doped binary GeO_2 – V_2O_5 glass system revealed that grape-like α-GeO_2 structures, blocky shaped β-GeO_2 structures and sphere-shaped V_2O_5 structures which are consisted with XRD results and with the erbium introduction to the system the new morphologies are observed on the SEM/SEI micrographs like needle like structures.

REFERENCES

Amato, G., Rossi, A. M., Boarino, L., Brunetto, N., 1997. On the role of germanium in porous silicon-germanium luminescence, *Philosophical Magazine Part B*, **76**, 395–403.

Balitsky, D. V., Balitsky, V. S.; Pushcharovsky, D. Yu,, Bondarenko, G. V., and Kosenko A. V., Growth and characterization of GeO_2 single crystals with the quartz structure, *Journal of Crystal Growth*, **180**, 212–219.

Bayya, S. S., Chin, G. D. , Sanghera, J. S. , Aggarwal, I. D., 2006. Germanate glass as a window for high energy laser systems,2006. *Optical society of America,* **14,** 24

Brown, M.E.,1998**.** Handbook of Thermal Analysis and Calorimetry, Volume 1: Principles and Practise ,Elseiver Science,Netherlands

Brown, M.E.,2001**.** Handbook of Thermal Analysis and Calorimetry, Volume 1: Application to inorganic and miscellaneous materials, Kluwer Academic Publishers, Dordrecht

Calas, G., Majerus, O., Cormier, L., Neuville, D. R., Galoisy, L., 2007. The structure of SiO_2–GeO_2 glasses: A spectroscopic study, *Journal of Non-Crystalline Solids*, **354**, 2004-2009

Cullity, B.D., 1956. Elements of X-ray Diffraction, Addison-Wesley Publishing Company, United States of America

Du, L.-S., Peng, L., and Stebbins, J. F., 2007. Germanosilicate and alkali germanosilicate glass structure: New insights from high-resolution oxygen-17 NMR, *Journal of Non-Crystalline Solids*, **353**, 2910–2918.

Egerton, R. F., 2005. Phyrical Principles of Electron Microscopy : An Intoduction to TEM, SEM, and AEM, Springer Science and Business Media, United States of America.

El-Mallawany, R., 2000. Structural Interpretations on tellurite glasses, *Materials Chemistry and Physics*, **63**,109-115

Gouveia-Neto, A. S., Bueno, L. A., do Nascimento, R. F., da Silva, E. A., and da Costa, E. B., 2009. 1540 nm fiber laser excited upconversion luminescence in erbium-doped lead–fluoride nanocrystals, *Journal of Non-Crystalline Solids*, **355**, 488–491.

Hannon, A. C., Martino D. D., Santos L. F., and Almedia R. M., 2007. A model for the Ge–O coordination in germanate glasses, *Journal of Non-Crystalline Solids*, **353**, 1688-1694.

Hatakeyamma, T., Liu, z., 1999. Handbook of Thermal Analysis, Wiley, Chichester

Henderson, G. S., 2007. The Germanate Anomaly: What do we know?, *Journal of Non-Crystalline Solids*, **353**, 1695-1704.

Hawkes, P.W., Spence J.C.H., 2007. Science of Microscopy, Springer Science and Business Media, United States of America.

Jerkins, R., Synder R.L., 1996. Introduction to X-ray Powder Diffractometry, John Wiley and Sons, Canada

Joubert, M. F., 1999. Photon avalanche upconversion in rare earth laser materials, *Optical Materials*, **11**, 181–203.

Kassab, L. R. P., Hora, W. G., Lozana, W. B., de Oliviera, M. A. S., and Maciel, G. S., 2007. Optical properties of Er^{3+} doped GeO_2–PbO glass: Effect of doping with Bi_2O_3, *Optics Communications*, **269**, 356–361.

Khan, M. N.,Khawaja, E.E.,Save, D., Kutub, A. A., Hogarth, C. A., 1984. Electrical Conductivity of Semiconducting V_2O_5-GeO_2 Glasses, *International Journal of Electronics,* **56**, 3, 395-401

Kissinger, H. E., 1965. Variation of Peak Temperature With Heating Rate in Differential Thermal Analysis, *Journal of Research of the National Bureau of Standards*, **57**, 217–221.

Khawaja, E. E., Tegally F., Hwang J. S., Li, A. S. W., Kutub, A. A., 1985. Effect of Annealing on the Electrical and Optical- properties of V_2O_5-GeO_2 Glasses, *International Journal of Electronics*, **56**, 3, 395-401

Klimesz, B., Dominiak-Dzik, G., Lisiecki, R., and Ryba-Romanowski, W., 2008. Systematic study of spectroscopic properties and thermal stability of lead germanate glass doped with rare-earth ions, *Journal of Non-Crystalline Solids*, **354**, 515–520.

Kobayasbhi, K., 2002. Development of infrared transmitting glasses, *Journal of Non-Crystalline Solids*, **316**, 403-406

Lezal, D., Pedlikova, J., Kostka, P., Poulain, M., and Zavadil, J., 2001. Heavy metal oxide glasses - preparation and physical properties, *Journal of Non-Crystalline Solids*, **284**, 288–295.

Lin, Q., Xia, H., Zhang, Y., Wang, J.,Zhang J.,, He S., 2007. Gain properties of germanate glasses singly doped with Tm^{3+} and Ho^{3+} ions, *Journal of Rare Earth*, **27**,76-82

Margaryan, A., and Piliavin M. C., 1993. *Germanate glasses: structure, spectroscopy and properties*, ARTECH HOUSE, INC., Boston.

Marinov, M., Krivoshieva, V., Stavrakieva, D., 1975. Phase-Equilibrium in GeO_2-V_2O_5 System, Dokladi Na Nolgarskata Akademiya Na Naukite **28**, 47-50

Memon, A., 1998. Preparation Effects on the Spectroscopic Properties of V_2O_5-GeO_2 Glass, *International Journal of Infrared and Millimeter Waves*, **9**,10,913-922

Micolaut, M., Cormier, L., and Henderson, G. S., 2006. The structure of amorphous, crystalline and liquid GeO_2, *Journal of Non-Crystalline Solids*, **284**, 288–295

Mortier M., 2003. Nucleation and anionic environment of Er^{3+} in a germanate glass, *Journal of Non-Crystalline Solids*, **318**, 56–62

Nie, Q., Lu, L., Dai, S., Xu, T., Shen, X., Zhang, X., Liang, X., and Zhang, X., 2007. Investigation of thermal stability and spectroscopic properties in Er^{3+} doped bismuth – boron – germanium glasses, *Physica B: Condensed Matter*, **392**, 195–199.

Niwa, K., Ikegaya, H., Hasegawa, M., Ohsuna, T., Yagi T., 2010. Submicron rectangular hollow tube crystals of rutile-type GeO_2, Journal of Crystal Growth 312, 1731-1735.

Öveçoğlu, M.L., Özen, G., Cenk, S., 2005. Microstructural characterization and crystallization behaviour of $(1-x)$TeO2–xWO3 (x = 0.15, 0.25, 0.3 mol) glasses, *Journal of the European Ceramic Society,* **26***,* 1149-1158

Öveçoğlu, M.L., Öz, B., Özen, G., Kabalcı, I.,2005. Microstructural characterization and crystallization kinetics of $(1-x)TeO_2$–xK_2O (x = 0.05, 0.10, 0.15, 0.20 mol) glasses, *Journal of the European Ceramic Society,* **27***,* 3239-3251

Özen, G., Tatar, D., Öveçoğlu, M.L., 2008. Microstructural characterization and crystallization of $(1-x)TeO_2$–$xCdF_2$ (x = 0.10, 0.15, 0.25 mol) glasses, *Journal of the European Ceramic Society,* **28***,* 3097-3106

Pal A., Maiti A., Mukherjee S., Basu C., 1996. Ultrasonic Study on Germanium-Rich Binary V_2O_5—GeO_2 Glass: Signature of Isopaustic Character, Journal of Materials Science Letters **15,**4,329-332

Prakapenka, V.P., Shen, G., Dubrovinsky, L.S., Rivers, M.L., Sutton, S.R., 2004. High pressure induced phase transformation of SiO_2 and GeO2: difference and similarity, *Journal of Physics and Chemistry of Solids*, **65**, 1537-1545

Saddeek, Yasser B, Shaaban, Essam R., Aly, Kamal. A., SAyed, I.M., 2009. Characterization of some lead vanadate glasses, *Journal of Non-Crystalline Solids* **352**, 160-166.

Sankarappa, T., Kumar, B.V., Kumar, M. P., Kumar, S., 2009. Electronic transport properties of mixed transition metal ions doped borophosphate glasses, *Journal of Non-Crystalline Solids*, **355**, 229–234.

Sharaf El-Deen, L. M., 2000. The ac conductivity studies for Cu_2O–Bi_2O_3 glassy system *Materials Chemistry and Physics*, **65**,275-281

Speyer, R.F., 1994. Thermal analysis of Materials, Marcel Dekker, United States of America

Stebbins, J. F.,Peng, L., 2007. Sodium germanate glasses and crystals: NMR constraints on variation in structure with composition, *Journal of Non-Crystalline Solids*, **353**, 4732-4742

Su, Q., Feng, L., Tang, Q., Liang, L., Wang, J., Liang, H., 2007. Optical transitions and up-conversion emission of Tm^{3+}-singly doped and Tm^{3+}/Yb^{3+}-codoped oxyfluoride glasses, *Journal of Luminescence,* **436**, 272–277

Su, Q., Feng, L., Tang, Q., Liang, L., Wang, J., Liang, L., 2006. Optical properties of Ho^{3+}- doped novel oxyfluoride glasses, *Journal of Luminescence,* **124**, 187–194

Trukhin, A., 2009. Luminescence of polymorph crystalline and glassy SiO_2,GeO_2: A short review, *Journal of Non-Crystalline Solids,* **355**, 1013-1019.

Tatar, D., Özen, G., Öveçoğlu, M.L.,Erim, B., 2008. Glass transition and crystallization of 0.8TeO2 + 0.2CdF2 glass , *Journal of the European Ceramic Society,* **29***,* 329-335

Url-1 < *http://www.msm.cam.ac.uk/phase-trans/2002/Thermal1.pdf*>, accessed at 29.06.2010

Url-2 < *http://web.mit.edu/3.091/www/archives/Notes_5.pdf* >, accessed at 12.07.2010

Url-3 < *http://www.phy.cuhk.edu.hk/course/surfacesci/mod5/m5_s3.pdf* >, accessed at 03.09.2010

Walsh, B. M., Barnes , N. P., Reichle , D. J., Jiang, S.,2006, Optical properties of Tm3+ ions in alkali germanate glass, 2006. *Journal of Non-Crystalline Solids*, **352**, 5344-5352

Wang, X., Wang, L.,Erwing, R. C., 2001. Ion irradiation-induced amorphization of two GeO_2 polymorphs, Nuclear Instruments and Methods in Physics Research **B 175-177**, 615-619

Wang, G., Xu, S., Yang, J., Dai, S., Lili,H., Jiang, Z., 2004. Thermal stability, spectra and laser propertiesof Yb: lead–zinc–telluride oxide glasses, *Journal of Non-Crystalline Solids*, **336**, 102-106

Wang, G., Nie, Q., Wang, X., Dai, S., Xu,T., Shen, X., Zhang, X., 2010. Research on the Novel $GeSe_2$–In_2Se_3–KBr Chalcohalide Optic Glasses, *Materials Research Bulletin*, **45**,1141-1144

Yamane, M., and Asahara, Y., 2000. *Glasses for photonics*, Cambridge University Press, Cambridge.

Zhang, J., Xu, R., Tian, Y., Wang, M., Hu, L., 2010. Investigation on broadband near-infrared emission and energy transfer in Er^{3+}–Tm^{3+} codoped germanate glasses, *Optical Materials.*

APPENDICES

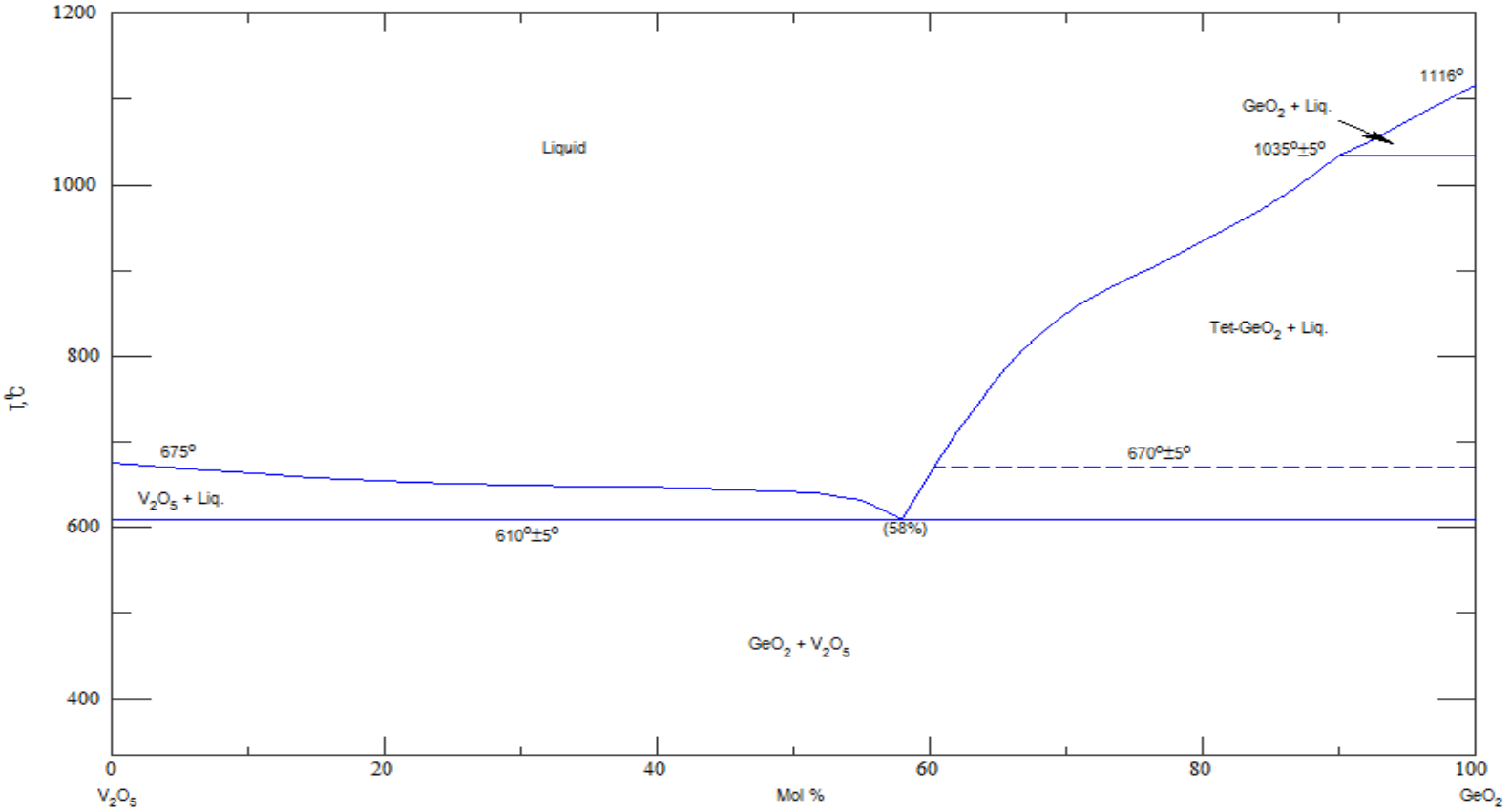

Figure A.1:System GeO_2-V_2O_5 (Marinov et al., 1975).

Table B.1 : All of the crystals structures, lattice parameters, space groups and card numbers of the crystalline phases

Crystal	Struct.	Space Group	a(nm)	b(nm)	c(nm)	β(°)	CN
α-GeO_2	Hex.	$P3_221$(154)	4.98502		5.648	90	36-1463
B-GeO_2	Tetra.	P42/mnm	4.4019	4.4019	2.8651	90	70-6994
V_2O_5	Orth.	Pmmn	11.516	3.5656	4.3727	90	41-1426

CURRICULUM VITAE

Candidate's full name	**:**	Deniz YILMAZ
Place and date of birth	**:**	İstanbul, 16.03.1984
Permanent Address	**:**	Kadıköy/İstanbul
Universities and Colleges attended	**:**	Yıldız Technical University Physics